Characteristics of in situ stress field in the Huainan mining area, China and its control factors

Xiuchang Shi (sxc@huel.edu.cn)
Henan University of Economics and Law
Jixing Zhang
Geological Survey of Jiangsu Province
Guoqing Li
China University of Geosciences

Research Article

Keywords: In situ stress, hydraulic fracturing, stress regime, geological structure, fault friction strength, Huainan mining area

Posted Date: March 4th, 2021

DOI: https://doi.org/10.21203/rs.3.rs-260973/v1

Characteristics of *in situ* stress field in the Huainan mining area, China and its control factors

Xiuchang Shi[1,5*] , Jixing Zhang[2], Guoqing Li[3,4]

[1] *BIM Technology and Intelligence Construction in Henan Engineering Laboratory, Henan University of Economics and Law, Zhengzhou 450046, P.R. China;*

[2] *Geological Survey of Jiangsu Province, Nanjing 210018, P.R. China;*

[3] *School of Earth Resources, China University of Geosciences, Wuhan, Hubei 430074, P. R. China;*

[4] *State Key Laboratory of Water Resource Protection and Utilization in Coal Mining, China Energy Investment Corporation Limited, Beijing 100011, P. R. China;*

[5] *College of Geosciences and Surveying Engineering, China University of Mining and Technology (Beijing), Beijing 100083, P. R. China.*

[*] Corresponding author, E-mail: sxc@huel.edu.cn (X. Shi)

Abstract : Due to the high *in situ* stresses, dynamic disasters occurred frequently in the Huainan mining area, China. While our understanding of the *in situ* stresses in this area is still insufficient. In this study, the *in situ* stresses of 18 sections in two boreholes in the Xinji No. 1 coalfield were measured by using hydraulic fracturing method, and the distribution of *in situ* stresses in the Huainan mining area were investigated. The relationship between *in situ* stress and geological structure in the Huainan mining area were summarized and the limitation of fault friction strength on *in situ* stresses were discussed. The result showed that the maximum horizontal principal stress (σ_H) at Xinji No. 1 mine was 13.95 - 25.23 MPa, the minimum horizontal principal stress (σ_h) was 12.16 - 21.17 MPa. The average azimuth of the maximum horizontal principal stress was N83.61 °E. The statistical results showed that the *in situ* stresses in Huainan mining area were characterized by a strike-slip faulting regime. Both the horizontal and vertical principal stresses increased approximately linearly with the increase of burial depth. The direction of the maximum principal stress in the study area is closely related to the tectonic movement and the ratio of maximum principal stress to minimum principal stress was primarily limited by the friction strength of fault. The outcomes of this research can provide some reliable engineering parameters and benefit the roadway layout and support design in the Huainan mining area.

Keywords: *In situ* stress; hydraulic fracturing; stress regime; geological structure; fault friction strength; Huainan mining area

Highlights:

(1) *In situ* stresses were measured at Xinji No. 1 mine in Huainan mining area.

(2) Regional *In situ* stress field of Huainan mining area was analyzed systematically.

(3) Influence of tectonic movement on *in situ* stress field was analyzed.

(4) Restraint mechanism of fault friction strength on *in situ* stress was revealed.

1. Introduction

In situ stress is the virgin stress that exists in the crustal rock mass and is the fundamental force that causes deformation and failure of surrounding rock in underground engineering excavation. Rock burst, coal and gas outburst events and large deformation of surrounding rock are more likely to occur in the presence of high *in situ* stresses (Shan and Yan, 2010; Xiao et al., 2016). Mastering the *in situ* stress state in the engineering area is a prerequisite for determining the mechanical properties of the engineering rock mass, analyzing the stability of surrounding rock, and realizing scientific design and decision-making of excavation in geotechnical engineering (Zoback et al., 1985). Field measurement of *in situ* stress is the most reliable way to accurately understand the distribution of *in situ* stress in the engineering area (Finkbeiner et al., 1997; Martin and Lanyon, 2003; Yaghoubi and Zeinali, 2009; Funato and Ito, 2017; Yang et al., 2017). In 1932, Liearace successfully performed the original rock stress measurement in the Hoover Dam discharge tunnel for the first time (Carder, 1945). In the late 1960s, Haimson and Fairhurst (1969) proposed the theory of *in situ* stress measurement by hydraulic fracturing. Brown and Hoek (1978) summed up the measurement results of *in situ* stress in different regions of the world in 1978, summarized the law of vertical stress varying with depth in various countries of the world, and drew the regression curve of the ratio of average horizontal *in situ* stress to vertical *in situ* stress varying with depth. Since the 1980s, dozens of countries in the world have carried out a variety of methods of *in situ* stress measurements, such as hydraulic fracturing, overcoring, borehole caving, and acoustic emission, which have been successfully applied in engineering application, earthquake prediction, oil and coal mining (Gay, 1975; Greiner, 1975; Cornet, 1984; Bell, 2006; Zhao et al., 2015; Oliver et al., 2018). Among them, hydraulic fracturing method is widely used one. *In situ* stress measurement and related research work in coal mines lags behind other industries. Mastering the distribution of *in situ* stress in coal mine areas is of great significance for safe and efficient coal and coal-bed methane extraction (Li et al., 2019). Kang et al. (2010) gathered a total of 204 stress measurement data by hydraulic fracturing in 49 coal mines within 13 Chinese coal mining areas to investigate the distribution characteristics of *in situ* stresses. Meng et al. (2011) analyzed the characteristics of *in situ* stress field and the relationship between permeability of coal reservoir and the *in situ* stress in the Southern Qinshui basin, China. Coggan et al. (2012) analyzed the effects of *in situ* stress on coal mine roadway stability by numerical modelling.

Paul and Chatterjee (2011) discussed cleat orientation and other structural features, observed in the outcrops of 14 major coal seams in Jharia coalfield of India and its directional relationship with the *in situ* stress orientation pattern.

The Huainan mining area in China is characterized by a great burial depth and complex mining conditions (Guo et al., 2012). With the increase of mining depth, most of the mines enter deep mining at the first level and all of them enter deep mining at the second level, with an average mining depth of 875 m. There is a high in situ stress level in the deep of this mining area. And disasters such as impact underground appearance, gas outburst and large deformation of roadway surrounding rock occur frequently, which seriously threaten the safety of mine production (Li et al., 2019; Li et al., 2013; Yang et al., 2012). Therefore, it is of great significance to investigate the distribution laws of the *in situ* stress and its control mechanism in the Huainan mining area for the safe and efficient coal mining. For a long time, many scholars have carried out *in situ* stress measurement in Huainan mining area and achieved some fruitful results. For instance, Han et al. (2008) measured the *in situ* stress in the Panji No. 1 mine and No. 2 mine by using hollow inclusion stress-relief method and analyzed the influence of *in situ* stress on coal and gas outbursts. Liu et al. (2012) used the hydraulic fracturing and stress relief methods to measure the *in situ* stress in Xie No. 1 mine, Pan No. 3 mine and Wangfenggang mine, and analyzed the characteristics of *in situ* stress field in the deep of the mining area.

Previously measured *in situ* stress data were rather scattered and are insufficient for the analysis of regional stress distribution. In this research, the hydraulic fracturing *in situ* stress measurement method was used to investigate the *in situ* stress state in Xinji No. 1 Mine. In combination with previously measured data, the distribution characteristics of the *in situ* stress in the Huainan mining area were statistically studied, and the influence mechanism of the geological structure on the *in situ* stress field was also discussed. This study can provide basis for the control of surrounding rock deformation and failure and the optimization of roadway support scheme in Huainan mining area.

2. Geological setting

The Huainan mining area is in the north central part of Huainan city Anhui province, China. It is one of China's 14 large-scale coal bases with a length of 140 km from east to west, a width of 20-30 km from north to south, and an area of 3200 km^2. In terms of regional geological structure, the Huainan mining area is located in the south edge of North China plate. It starts from Tanlu fault in the east, ends at Fuyang fault in the west, connects with Bengbu uplift in the north, and adjoins with Hefei depression in the south. The Huainan coal field is in the form of compound syncline, with the main structure in the northwest direction. The two flanked low

mountains include the Proterozoic Wuhe group, Fengyang group, Bagongshan group of Qingbaikou system, Paleozoic Cambrian and Ordovician. The axis has a secondary wide and gentle fold, mainly composed of Carboniferous and Permian coal-bearing strata, and the overlying Cenozoic has a general thickness of 200-500m. There are Fufeng and Shungengshan thrust nappes in the south and Minglongshan-Shangyao gravity slip structures in the north. The NNE-trending regional faults are superimposed on the NW trending main structural line (Fig. 1).

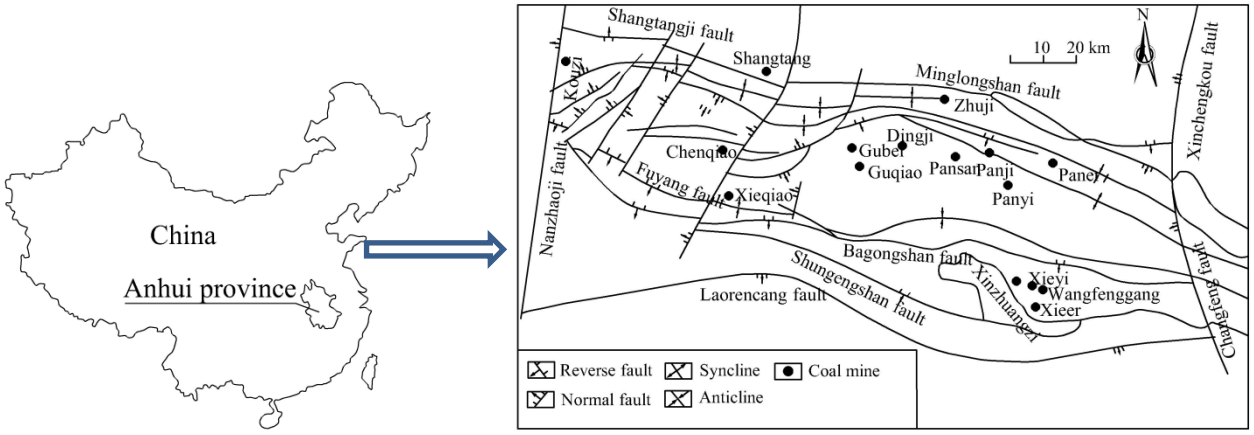

Fig.1. Geological structure diagram of the Huainan mining area in Anhui province.

The north and south wings of the compound syncline are well-developed, showing a thrust nappe from south to north, and forming the nappe structure pattern of the two wings. The Shungengshan fault and Fuyang-fengtai fault on the south wing constitute Shungengshan, Bagongshan and Liuzhuang nappes from south to north. The Shangyao-Minglongshan-Shangtang fault on the north wing forms a north-south sliding nappe. In the compound syncline, reverse faults in the striking direction and NNE normal fault in the dipping direction are developed, the latter is close to eastern and western structure belt, mainly including the Wudian fault, Xinchengkou-Changfeng fault, Chenqiao-Yingshang fault, Koziji (Xifanlou) fault, etc., forming a group of ladder structures which are generally parallel to the Tanlu fault and inclines to the west. Studies have shown that near EW-trending folds and fault structures in the Huainan coalfield were mainly formed in the Indosinian and Yanshan periods, while some normal faults in the NNE direction were mostly new structures and formed in the Himalayan movement period.

The Xinji No. 1 Mine is located in the middle section of the Xieqiao syncline flank of the Huainan complex syncline and the Yingfeng-Fufeng nappe structure. The overall structural form in this mine is that the Fufeng thrust fault pushes the foreign system from south to north over the *in situ* system (coal-bearing stratum). Affected by a strong compressive stress from south to north, the overlying branch fault form of the Fufeng nappe

structure has undergone a full nappe, forming a shingle fan structure combination. The main fold structures in this mine include the Xieqiao syncline, Liuka anticline and Qiandaliujia syncline. The main faults include the reverse fault group formed by the North-South compression of Fufeng nappe and the F10 normal fault group formed by the nearly east-west extension (Fig. 2).

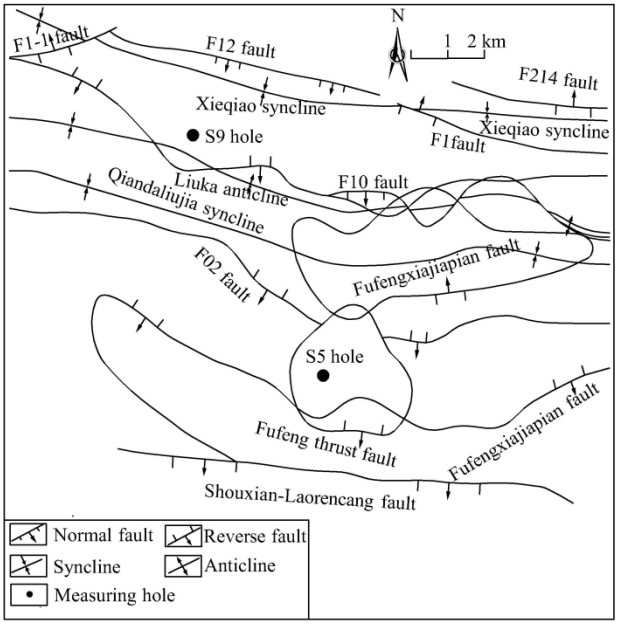

Fig.2. Geological structure in the Xinji No.1 coal mine.

3. *In situ* stress measurement method by hydraulic fracturing

3.1. Basic theory of hydraulic fracturing

Fracturing pressure during hydraulic fracturing is an important parameter and it can be expressed as follows (Haimson, 1978):

$$P_{\mathrm{b}} = 3\sigma_h - \sigma_H - p_p + T_0 \tag{1}$$

Where P_{b} is the strata breakdown pressure when the stratum is hydraulically fractured; p_p is the pore pressure; T_0 is the rock tensile strength; σ_h and σ_H are the minimum and maximum horizontal principal stresses acting on the cross section of borehole, respectively.

After the fracture of the borehole wall, if the injection continues to increase the pressure, the fracture will extend deep into the wall rock. If the injection stops and the fracturing circulation system keeps sealed, the fracture will stop extending immediately and tend to close. The equilibrium pressure that can keep the fracture open is called instantaneous shut-in pressure (P_s), which is equal to the minimum principal stress perpendicular

to the fracture plane; i.e.

$$P_s = \sigma_h \tag{2}$$

If the sealing section is pressurized again to reopen the fracture, the fracture reopening pressure (P_r) can be obtained. Since the rock has been broken, the tensile strength (T_0) is equal to zero. P_r can be obtained as follows:

$$P_r = 3\sigma_h - \sigma_H - p_p \tag{3}$$

Combining Eq. (1) with Eq. (3), The tensile strength of rock (T_0) can be obtained as follows:

$$T_0 = p_b - p_r \tag{4}$$

Combining Eq. (2) with Eq. (3), the maximum horizontal principal stress (σ_H) can be estimated as follows:

$$\sigma_H = 3p_s - p_r - p_p \tag{5}$$

The vertical principal stress can be estimated according to the gravity of overlying strata, i.e.

$$\sigma_V = 0.023H \tag{7}$$

Where σ_v is the vertical principal stress; H is the occurrence depth of the rock mass.

3.2. Measurement equipment and method

3.2.1. Measurement equipment of *in situ* stress

Sy-2007 single-loop *in situ* stress measurement system was adopted for the *in situ* stress measurement, as shown in Figure 3. The single circuit was to use an independent pressurization system to pressurize the packer and test section, which was characterized by only using a high-pressure pipe to pressurize the downhole during the measurement process, and the downhole was converted by push-pull switch to seal the packer and fracture the well section respectively.

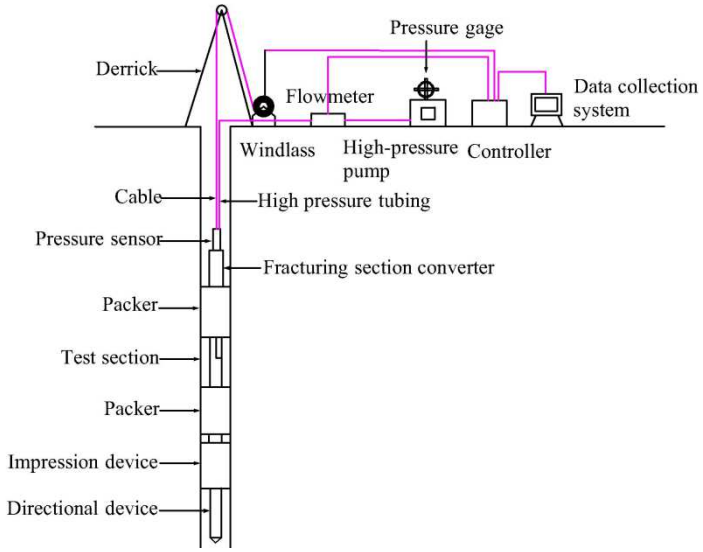

Fig. 3. Sketch of single loop hydraulic fracturing *in situ* stress measurement system.

Sy-2007 hydraulic fracturing *in situ* stress measurement system is specially used for *in situ* stress measurement. The system is composed of an LSJ-4×400 high pressure oil pump, an ACP-4001 industrial control desktop computer, a control box, a push-pull switch, a directional device, packers, an impression device and high-pressure oil pipes. That is, it is a relatively complete measurement system. The control and data recording system are equipped with the following hardware: a field data processing computer, a multi-channel data acquisition card and a recoding and processing code of hydraulic fracturing parameters.

3.2.2. *In situ* stress measurement method

(1) Hydraulic fracturing *in situ* stress measurement program

Hydraulic fracturing *in situ* stress measurement method has the follow procedures: a pair of expandable packers were used to seal a section of borehole at a selected measurement depth, and then the test section (often called the fracturing section) was pressurized by pumping fluid. At the same time, the data acquisition was used to record the pressure variation over time. Based on the analysis of the measured curves, the characteristic pressure parameters could be obtained. Then, according to the theoretical calculation formulas, the maximum and minimum horizontal principal stress values at the measurement point and the rock mechanical parameters such as the hydraulic fracturing tensile strength of the rock could be obtained (Hubbert and Willis, 1957).

The specific test procedure of hydraulic fracturing method is as follows: ① drill to the measuring position and isolate the test section with two packers; ② inject high-pressure water into the isolation section until a significant fracture appears in the hole wall. The water pressure at this time is called the breakdown pressure, P_b.

Then, continue to raise water pressure to expand the fracture. When the fracture extends to 2 ~ 3 times of the borehole diameter, close the high-pressure water system. At this time, the constant water pressure is called the closing pressure, which is recorded as P_s. Finally, the pressure is released to close the fracture; ③ re-inject high-pressure water into the sealing section to reopen the fracture, and record the pressure when the fracture reopens, which is recorded as P_r. This re-pressurization process is repeated 3 times; ④ take the packer out of the borehole after the packer is completely depressurized; ⑤ the impression device wrapped with a special rubber is sent into the fracture section and pressurized to make the shape, size, orientation of the hydraulic fracture crack and the original joint cracks in the hole wall are recorded by the rubber impression. A typical pressure-time curve obtained during hydraulic fracturing is shown in Fig. 4.

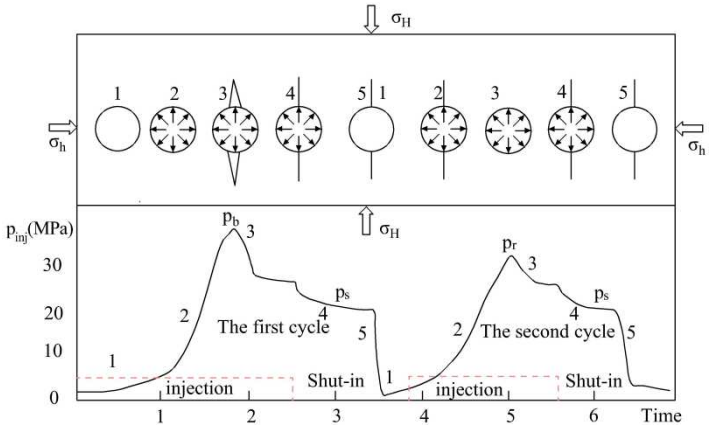

Fig. 4. Typical fracturing process curve of hydraulic fracturing stress measurement.

(2) Impression orientation test method

Test method for moulage and orientation: the fracture orientation could be determined after the fracturing measurement in the isolation section to determine the direction of the maximum horizontal principal compressive stress. The method used in this test is the directional impression method. The directional impression system could directly print the crack marks on the hole wall. It consisted of an automatic orientation instrument and an impression device. When determining the orientation of hydraulic fracture plane, firstly, place the impression device connected to the orientation device to the depth of the hydraulic fracturing stress measurement section, and then expand the impression device on the ground through a pressurization system. In order to obtain clear crack marks, it was necessary to apply enough high pressure to cause the existing fractures in the hole wall to re-open to allow the semi-vulcanized rubber to squeeze in and maintain the corresponding time. When the pressure holding time was over, the pressure on impression device was removed and the device was put out of the hole. There were traces of fractures on it. In general, the hydraulic fracture was a group of

radial relative longitudinal cracks, which could be easily identified. According to the relationship between the magnetic compass pointer of the director and the baseline marked on the impression device, the orientation of the fracture surface was calculated. Namely, the orientation of the maximum horizontal principal stress was obtained.

(3) Identification of instantaneous shut-in pressure

In the *in situ* stress measurement by the hydraulic fracturing method, the minimum principal stress is equal to the fracture closing pressure Ps. The closing pressure identification method determines the reliability of the minimum principal stress measurement results. The problem of fracturing fluid leakage caused by formation permeability is likely to cause difficulty in identifying the closing pressure point on the hydraulic fracturing test curve. For this reason, related researchers have conducted profound research and proposed a variety of methods to identify closure pressure. In this test, a single tangent method is used to accurately identify the instantaneous shut-in pressure. This method is to make a straight line (tangent line) tangent to the descent curve from the point of pump shut-off. The point where the tangent leaves the descent curve is the instantaneous shut-in pressure point. In the strike-slip faulting regime, the minimum horizontal principal stress is equal to the instantaneous shut-in pressure *P*s.

3.3. Arrangement of *in situ* stress measuring points

Combined with the progress of exploration project of Xinji No.1 mine, S5 borehole and S9 borehole for hydrogeological supplementary exploration of Shanxi formation were selected as the measurement boreholes for hydraulic fracturing. The wellhead elevation and depth of S5 borehole were 26.16 m and 656.70 m respectively. The wellhead elevation and depth of S9 borehole were 23.27 m and 928.86 m respectively. According to the specific geological and lithological conditions of the borehole, considering the actual needs of the project, ten sections were tested in S5 borehole, which were at depths of 440m, 470m, 485m, 512m, 540m, 560m, 580m, 600m, 620m, and 640m, respectively; eight sections were tested in S9 borehole, which were at depths of 500m, 535m, 580m, 665m, 715m, 790m, 820m and 845m, respectively. To reveal the *in situ* stress distribution around the roadway, these test points were arranged as far as possible in the sandstone sections at the top and bottom of the coal mine roadway.

3.4. *In situ* stress measurement results

Through hydraulic fracturing *in situ* stress measurement, fracturing curves of *in situ* stress measurement in Xinji No.1 mine were obtained. The fracturing curves of the first and fifth sections of S5 borehole and the fourth

and sixth sections of S9 borehole are shown in Fig. 5-8. According to the obtained data, the data quality of each section was satisfactory. The pressure record curves were quite standard with obvious peak values of fracture pressure and the regularity of each cycle were very strong. The fracture parameters measured by each cycle had good consistency, therefore the *in situ* stress data of each measuring point was reliable.

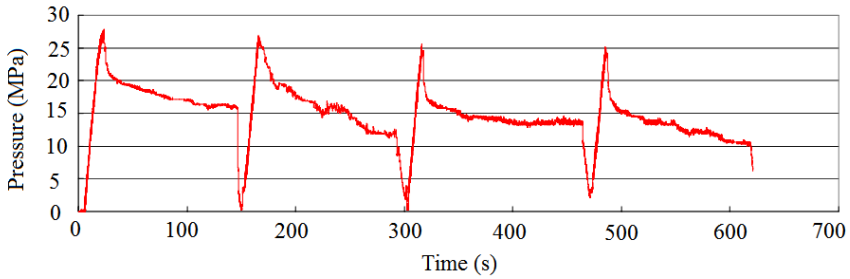

Fig. 5. Pumping pressure versus test time at the depth of 439.5-440.5 m in S5 hole.

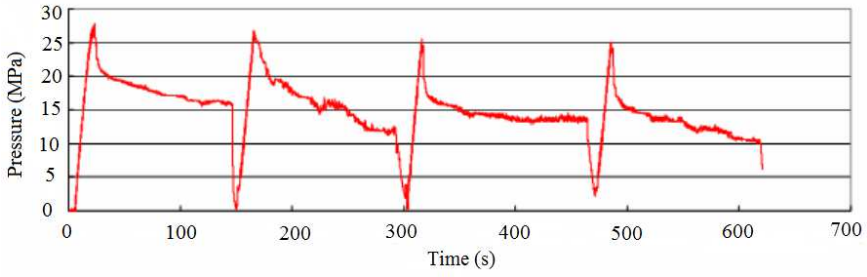

Fig. 6. Pumping pressure versus test time at the depth of 539.5-540.5 m in S5 hole.

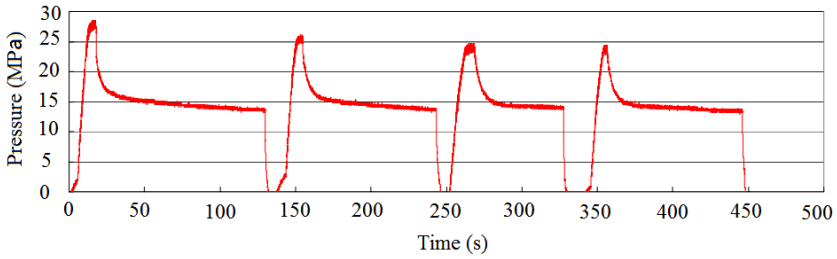

Fig. 7. Pumping pressure versus test time at the depth of 664.5-665.5 m in S9 hole.

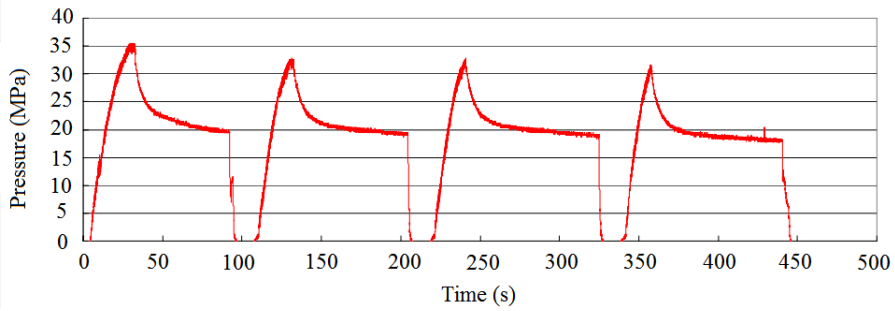

Fig. 8. Pumping pressure versus test time at the depth of 789.5-790.5 m in S9 hole.

According to the collation and calculation analysis of the test data, the breakdown pressure (P_b), fracture

reopening pressure (P_r), instantaneous shut-in pressure of the hydraulic fracture plane (P_s), rock pore pressure (P_p) and tensile strength T_0 of rock were determined for each test section.

According to the measured pressure parameters and eqs. (1)-(7), the maximum and minimum horizontal principal stress values and vertical principal stress values were obtained, as shown in Table 1.

Table 1

In situ stress measurement results by hydraulic fracturing in the Xinji No.1 mine.

Survey section number	Depth (m)	Fracturing characteristic parameters					Principal stress value (MPa)			Orientation of maximum horizontal principal stress
		P_b	P_s	P_r	T	P_0	σ_v	σ_H	σ_h	
S5-1	440	22.90	12.15	19.00	3.89	4.35	13.20	13.10	12.15	
S5-2	470	25.79	13.52	21.85	3.94	4.70	14.10	14.01	13.52	NE86.7°
S5-3	485	25.78	13.57	21.58	4.20	4.85	14.55	14.28	13.57	
S5-4	512	24.67	14.82	24.34	0.33	5.12	15.36	15.00	14.82	
S5-5	540	27.56	15.64	25.4	2.16	5.40	16.20	16.12	15.61	NE67.2°
S5-6	560	26.31	15.06	23.08	3.23	5.60	16.80	16.50	15.06	
S5-7	580	27.5	17.55	26.63	0.87	5.80	17.40	20.22	17.55	
S5-8	600	28.6	18.01	26.21	2.39	6.00	18.00	21.82	18.01	NE92.3°
S5-9	620	29.83	19.91	29.38	0.45	6.20	18.60	24.15	19.91	
S5-10	640	28.57	19.24	26.49	2.08	6.40	19.20	24.83	19.24	NE79.8°
S9-1	500	18.90	12.16	16.68	2.19	5.00	15.00	14.80	12.16	
S9-2	535	25.79	15.52	22.49	3.30	5.35	16.05	18.72	15.52	NE66.10°
S9-3	580	28.78	15.57	23.18	5.60	5.80	17.40	17.73	15.57	
S9-4	665	29.67	17.82	25.34	4.33	6.65	19.95	21.47	17.82	
S9-5	715	35.69	20.64	32.1	3.59	7.15	21.45	22.67	20.64	NE89.20°
S9-6	790	35.31	21.16	31.08	4.23	7.90	23.70	24.50	21.16	
S9-7	820	35.5	22.3	34.03	1.47	8.20	24.60	24.67	22.30	
S9-8	845	36.6	23.1	35.21	1.39	8.45	25.35	25.64	23.10	NE102.30

In order to determine the orientation of the principal stresses, according to a comprehensive analysis of the fracturing test curves of S5 borehole, four measurement sections at depth of 469.5-470.5 m, 539.5-540.5 m, 599.5-600.5 m, and 639.5-640.5 m were selected for impression and orientation. The moulage and orientation measurement results are shown in the circle development diagram (Figure. 9). The rupture morphology of the four measurement sections are all upright cracks. According to a set of radially opposite longitudinal cracks, the fracture surface directions of the four measurement sections are N86.1 ° E, N67.2 ° E, N92.3 ° E and N79.8 ° E, the measured average maximum horizontal principal stress direction is N81.35 ° E, near the EW direction.

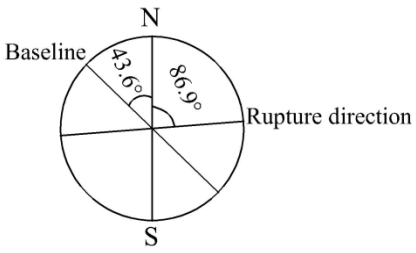

(a) Depth of 469.5-470.5 m

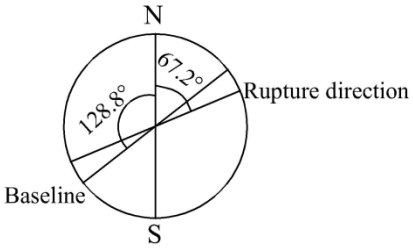

(b) Depth of 539.5-540.5 m

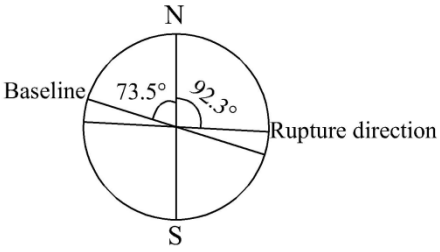

(c) Depth of 599.5-600.5 m

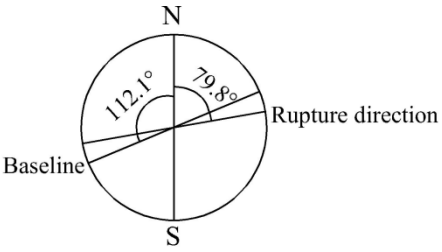

(d) Depth of 639.5-640.5 m

Fig. 9. Orientations of the observed hydraulic fractures in Hole S5 injection test in four depth intervals.

Through a comprehensive analysis of the fracturing test curves of the S9 hole, three measurement sections at depths of 534.5-535.5 m, 714.5-715.5 m, and 844.5-845.5 m are selected for impression measurement. The impression test results of the three sections are shown in Fig. 10.

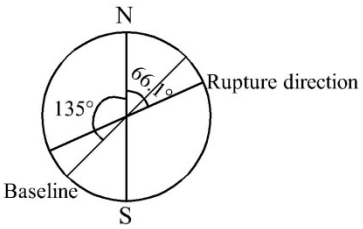

(a) Depth of 534.5-535.5 m

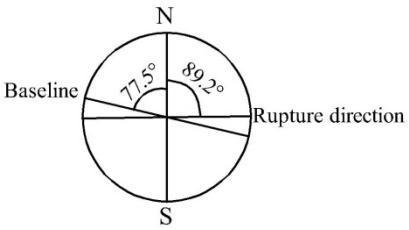

(b) Depth of 714.5-715.5 m

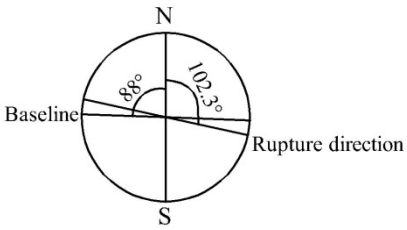

(c) Depth of 844.5-845.5 m

Fig. 10. Orientations of the observed hydraulic fractures in Hole S5 injection test in four depth intervals.

In conclusion, the maximum horizontal principal stress of Xinji No.1 mine was 13.95-25.23 MPa, and the minimum horizontal principal stress was 12.16-21.17 MPa. The average azimuth of the maximum horizontal principal stress in Xinji No. 1 mine was N83.61° E, that is, near EW direction.

4. Characteristics of *in situ* stress field in Huainan mining area

Based on the *in situ* stress measurements in Xinji No. 1 mine, a total of 76 sets of *in situ* stress data from the Pan No. 1 mine, Pan No. 2 mine, Xinzhuang mine, Guqiao mine and Wangfenggang mine in the Huainan mining area are further collected to systematically analyze the characteristics of *in situ* stress field.

4.1. Type and magnitude of *in situ* stress field

Among the 76 measuring points in Huainan mining area, 46 measuring points belong to the type of $\sigma_H>\sigma_v>\sigma_h$, accounting for 60.5% of the total measuring points; 11 measuring points belong to the type of $\sigma_v>\sigma_H>\sigma_h$, accounting for 14.4% of the total measuring points; 19 measuring points belong to the type of $\sigma_v>\sigma_H>\sigma_h$, accounting for 25% of the total measuring points. 57 measuring points have a maximum horizontal principal stress greater than the vertical principal stress, which accounts for 75% of the total measuring points. Therefore, the *in situ* stress field in Huainan mining area is dominated by horizontal stress, that is, horizontal tectonic stress predominates. The overall stress field is characterized by $\sigma_H>\sigma_v>\sigma_h$.

According to the stress magnitude, the stress can be classified into four different levels: a low stress level with a stress magnitude of 0-10 MPa, a medium stress level of 10-18 MPa, a high stress level of 18-30 MPa and a ultra-high stress level of greater than 30 MPa. Among the 76 measure points, 48 measuring points have a maximum horizontal principal stress of 18 MPa$\leqslant\sigma_H\leqslant$30MPa, and 6 points have a maximum horizontal principal stress of greater than 30 MPa and most of these points have a burial depth of greater than 550 m. 22 measure points with a burial depth of less than550m have a maximum horizontal principal stress of less than 18MPa. Therefore, the deep *in situ* stress state of Huainan mining area generally belongs to a high stress level.

4.2. Variation of horizontal and vertical principal stress with depth

The variation relationship between *in situ* stress and depth of each measuring point within 350.7-1150 m is shown in Fig. 11. In order to analyze the linear correlations between the vertical principal stress, the horizontal principal stress and the buried depth, a least square method is used for regression analysis, and the R test is used to test the significance of the regression curve.

Regression analyses show that the relationship between in situ stresses and burial depth in Huainan mining area can be expressed:

(1) Vertical principal stress:

$$\sigma_v=0.0232H+2.2837 \quad (8)$$

The significance test of the regression curve is performed: the number of samples is n=76, and the fitting goodness R^2=0.9145. It shows that there is a good linear correlation between the vertical principal stress and the depth.

(2) Maximum horizontal principal stress:

$$\sigma_H=0.0203H+6.4995 \quad (9)$$

The fitting goodness R^2=0.6916>R_{α}=0.290，α=0.01. It shows that there is a roughly linear correlation between the maximum horizontal principal stress and the depth.

(3) Minimum horizontal principal stress

$$\sigma_h=0.0145H+5.2348 \quad (10)$$

The fitting goodness R^2=0.6051> R_{α}=0.290，$\alpha = 0.01$. It shows that there is a roughly linear between the minimum horizontal principal stress and the depth.

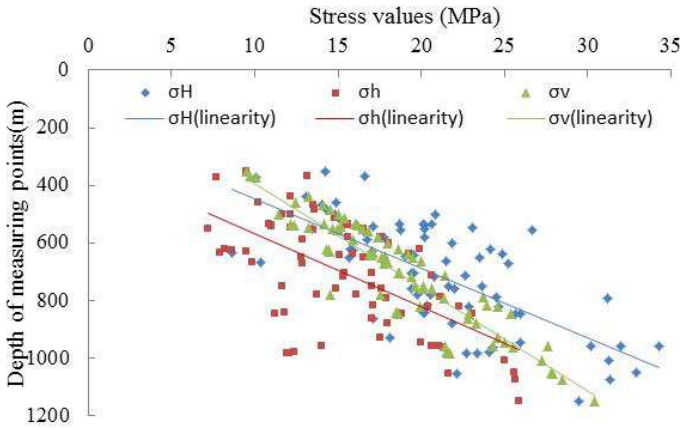

Fig.11. Variation of *in situ* stress values with depth in Huainan mining area.

It can be seen from Figure 11 that the maximum and minimum horizontal principal stresses and vertical principal stresses generally increase with the increase in depth. However, due to the great difference in geological structure, stratigraphic configuration, ground temperature and groundwater, there is a certain discreteness in the measurement data of *in situ* stress, especially the discreteness of the minimum horizontal principal stress.

4.3. Relationship between lateral pressure coefficient (λ) and depth

The lateral pressure coefficient (λ) is the ratio of the maximum horizontal principal stress to the vertical principal stress, which is an index reflecting the level of tectonic stress. The relationship between λ and depth is shown in Fig. 12. It can be seen that λ is rather discrete. At burial depths of less than 550 m, λ has the largest discretization range, but with the increase of burial depth, the discretization range of λ tends to decrease gradually. In Huainan mining area, λ values of 76 measuring points range from 0.505 to 1.822, among which 19 measuring points with $\lambda \leqslant 1.0$, account for 25% of the total number of measuring points, and 57 measuring points with λ> 1.0, accounting for 75% of the total number. It shows that the state of *in situ* stress in the mining area is dominated by horizontal stress, and the *in situ* stress field in the mining area is dominated by tectonic

stress field. With the increase of depth, the lateral pressure coefficient is close to 1.0. According to classification of the macro type of the original rock stress field (Peng and Yu, 1998), it can be found that the *in situ* stress field in the depth of −550m~ −1200 m in Huainan mining area is of geodynamic stress field type, but with the increase of the depth, it transforms into a quasi-hydrostatic pressure field type gradually.

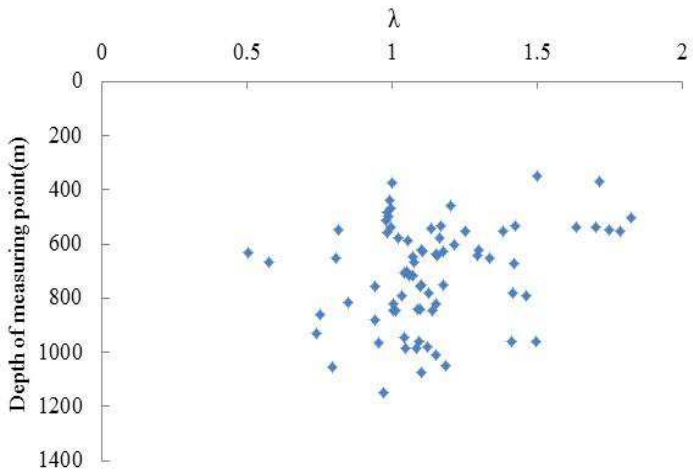

Fig. 12. Ratio of minimum horizontal principal stresses to vertical principal stresses with depth.

The lateral pressure ratio (κ) is the ratio of the average horizontal principal stress to the vertical principal stress, which can be described below:

$$\kappa = \frac{\sigma_H + \sigma_h}{2\sigma_V} \tag{11}$$

From the measured data of 76 measurement points, the variation range of κ is 0.485-1.535, and the distribution is relatively discrete. The variation range of κ is high at depths of less than 550 m and then decreases gradually with increase of burial depth with k approaching to 1.0 (Fig. 13). The variation curve of lateral pressure ratio with depth is in the inner and outer envelopes of Hoek-Brown (Hoek, 1990).

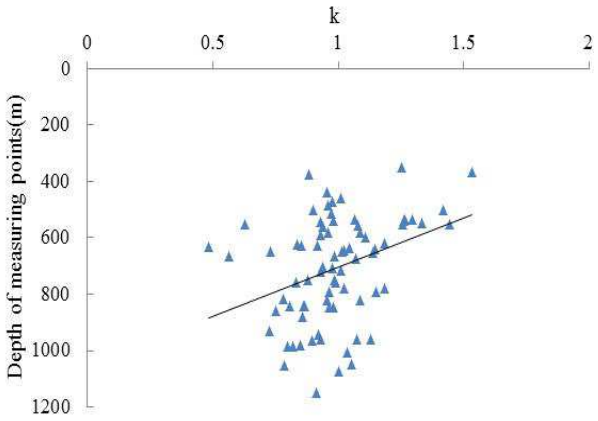

Fig.13. Ratio of average horizontal principal stress to vertical stress vs depth.

4.4. Ratio of maximum to minimum horizontal principal stresses

The ratio of the maximum horizontal principal stress to the minimum horizontal principal stress in Huainan mining area ranges from 1.004 to 2.275 (Fig. 14). According to the rock mechanics theory, the maximum shear stress is half of the difference between the maximum and the minimum principal stress, and the failure of rock mass is usually caused by shear failure. Therefore the ratio of maximum to minor horizontal principal stress, to a certain extent, reflects that the effect of tectonic stress in the mining area is relatively constant.

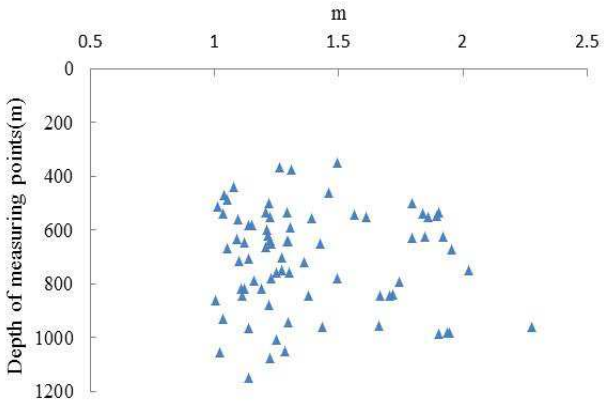

Fig. 14. The ratio of maximum to minor horizontal principal stress varying with depth.

4.5. Direction of maximum horizontal principal stress

Among the 76 groups of *in situ* stress data collected, 42 groups have measured the maximum horizontal principal stress direction. Influenced by the geological structure, the maximum horizontal principal stress direction is shown in the NE and NW directions, with 66.6% in the direction of NEE. Therefore, the dominant direction of the maximum horizontal principal stress in Huainan mining area is in the NEE direction, which is close to the EW direction. The coal-bearing strata in the Huainan mining area are mainly affected by compressive stress in the EW direction.

5. Influence of tectonic movement on *in situ* stress

Tectonic movement is the main cause of *in situ* stress field, especially in the horizontal direction. The current state of *in situ* stress is mainly controlled by the latest tectonic movement, but also is related to the tectonic movements occurred in the geological history.

In the geological history, the strata in Huainan mining area mainly experienced three major tectonic movements, including the Indosinian movement in the late Triassic, the Yanshan movement in the Mesozoic and the Himalayan movement in the Cenozoic. In the first stage, a series of EW direction compressional and torsional thrust faults and imbricated structures were formed in the south of the mining area under the action of

compressive stress in the SN direction, and "X" type joints in NW and NE directions were generated in the syncline. The maximum principal stress was in the SN direction. In the second period, the strata were compressed laterally in the NW-SE direction and twisted to the left by NE-NNE spinning. Except for the further development of faults and folds in the near EW direction, the structural differentiation was more obvious. The structures in the sub-EW direction were transformed into ones in the NWW-SEE direction, and a new fracture system was formed in this direction. The maximum principal stress was in the NWW-SEE direction. In the third period, the tectonic stress field was transformed from compression to extension. Under the action of tensile stress in the NWW-SEE direction, a large number of normal faults in the NWW-SEE direction were formed. At the same time, the stress field under the right-handed couple action in the sub-NE direction was formed, and the maximum principal stress was in the NEE-EW direction.

According to a large number of *in situ* stress measurement data, the orientation of the maximum horizontal principal stress in the Huainan mining area is primarily in the NEE-EW direction. This shows that the current *in situ* stress field in the mining area basically inherits the third stage tectonic stress field. The maximum principal stress of the tectonic stress field is in the NEE-EW direction. For example, the maximum horizontal principal stress of seven survey sections in Xinji No. 1 Mine is in the direction of NE83.61 °, which is the in sub-EW direction. This result is consistent with the direction of the tectonic stress field analyzed above. The results of *in situ* stress measurement in Xinji No. 1 mine further confirmed the mechanical genetic mechanism of the tensile-torsional fractural structures in Huainan mining area. The good agreement between the two shows the accuracy of the measurement results of the *in situ* stress field in this mine.

6. Constraint mechanism of fault friction strength on *in situ* stress

Tectonic movement has a clear controlling effect on the direction of the *in situ* principal stress, but the limiting conditions for the magnitude of the *in situ* stress are unclear, and it is a question worth considering. In essence, the magnitude of the *in situ* stress in the crustal rock mass is the result of the constraint of the frictional strength of discontinuities such as faults and cracks. Therefore, it is necessary to clarify the frictional strength of the fault and its constraint mechanism on the *in situ* stress. On this basis, the limit of *in situ* stress by the F10 fault in Xinji No.1 mine is analyzed.

6.1. Fault friction strength

Friction strength is a basic mechanical property of faults. Byerlee (1978) summarized a large number of experimental data of different types of rocks and faults, and found that under the action of high normal stress

($\sigma_n \geq 10\text{MPa}$), the friction of fault surface has nothing to do with surface roughness, normal stress, sliding speed, etc., and the friction coefficient (μ) fluctuates in a small range, i.e. $0.6 \leq \mu \leq 1.0$. The frictional strength of a fault is one of the mechanical properties of the fault. It is the shear stress of the fault during frictional sliding under the condition of *in situ* stress.

The test results show that the materials in the fault-affected zone are mainly composed of fault breccia and mylonitic debris (Logan et al., 1992). The measured density of the samples is 1.5g/cm^3-2.3g/cm^3, the uniaxial compressive strength is 0.51-0.65 MPa, the elastic modulus is 66.4-101.4 MPa, and the Poisson ratio is 0.37-0.38. The materials in the fault zone are characterized by extremely low mechanical strength and rigidity, obvious Poisson effect, and easy deformation.

Table 2 shows the tangent stiffness, normal stiffness and the friction coefficient of some structural planes in the sedimentary rock mass (Li and Yang, 1999). Cohesion C of different types of structural planes is very low, and tangential stiffness is less than normal stiffness. For sedimentary structural planes, due to different lithology characteristics of the upper and lower layers, normal deformation and shear deformation of structural planes are affected, and the friction coefficient of fracture structural planes is about 0.6. Sedimentary rock mass is prone to tensile failure or shear failure in the direction perpendicular to the structural plane.

Table 2

Mechanical parameters of some structural planes in sedimentary rock mass.

Structural Plane	Tangential stiffness k_s (MPa·cm^{-1})	Normal stiffness k_n (MPa·cm^{-1})	Cohesion C (MPa)	Friction coefficient
Limestone and coal seam	2.45	9.81	0.20	0.58
Coal seam and shale	1.47	5.88	0.10	0.58
Shale and sandstone	1.47	5.88	0.10	0.58
Faults filled with clay, weathered palisades	5.00	15.00	0.00	0.65
Filled with clay faults, slightly weathered palisades	8.00	18.00	0.00	0.75

6.2. Restriction of fault friction strength on *in situ* stress

Discontinuity surfaces, such as faults, folds and joints of different scales and in different directions are widely distributed in the coal mining area, and the magnitude of *in situ* stress is obviously constrained by the friction strength of these discontinuities (Zoback, 2007). The *in situ* stress values measured in many areas are balanced with the friction strength of discontinuities and therefore the *in situ* stress values can be inferred. However, it can't be simply considered that this is always the case. In fact, the *in situ* stress values of mining area can't exceed the friction strength of the primary fault. Fig. 15 gives an understanding of this concept.

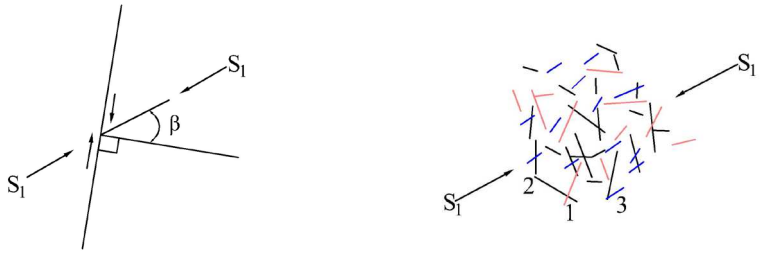

(a) Fault slip occurred in the dominant direction.

(b) There are faults in various directions in the formation, and some of them are in the dominant direction where sliding occurs.

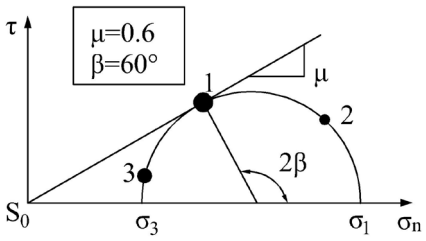

(c) Mohr circles for faults in different directions.

Fig. 15. Limiting diagram of fault frictional strength on *in situ* stress.

Fig. 15 (a) shows a two-dimensional fault. Ignoring the effect of the intermediate principal stress, and setting the angle between the fault normal and the maximum principal stress (S_1) as β , the shear and normal stresses acting on the fault plane can be expressed by the following equations:

$$\left.\begin{aligned} \tau &= 0.5(\sigma_1 - \sigma_3)\sin 2\beta \\ \sigma_n &= 0.5(\sigma_1 + \sigma_3) + 0.5(\sigma_1 - \sigma_3)\cos 2\beta \end{aligned}\right\} \tag{12}$$

Where σ_1 and σ_3 are the maximum and minimum effective principal stresses, respectively, $\sigma_1 = S_1 - P_p$,

$\sigma_3 = S_3 - P_p$; S_1 and S_3 are the maximum and minimum principal stresses, respectively; P_p is the pore pressure.

The faults (No.1) indicated by red line in Fig. 15 (b) are in the dominant direction. The faults (No.2) represented by the black line are nearly perpendicular to S_1, with larger normal stress and smaller shear stress. The faults (No.3) represented by the blue line are nearly parallel to S_1, and its normal stress and shear stress are smaller than those in the dominant direction.

For any given σ_3, there is a maximum value of σ_1 determined by the friction strength of the fault. Mohr circle cannot exceed the upper limit of the friction strength, as shown in Fig. 15 (c). The critical friction angle β in which the fault is the easiest to slide can be expressed as:

$$\beta = \frac{\pi}{4} + \frac{1}{2}\tan^{-1}\mu \tag{13}$$

According to Amonton's friction theorem (Archie 1950), Eq. (12) can be written as:

$$\frac{\sigma_n}{\tau} = \frac{\left(\frac{\sigma_1}{\sigma_3}+1\right)+\left(\frac{\sigma_1}{\sigma_3}-1\right)\cos 2\beta}{\left(\frac{\sigma_1}{\sigma_3}-1\right)\sin 2\beta} = \frac{1}{\mu} \tag{14}$$

Jaeger (1971) found that when the fault in the critical friction direction is in a limit friction equilibrium state, the relationship between the ratio of the maximum to the minimum effective principal stress and the fault friction coefficient can be expressed as follows:

$$\frac{\sigma_1}{\sigma_3} = \frac{S_1 - P_p}{S_3 - P_p} = [(\mu^2+1)^{1/2} + \mu]^2 \tag{15}$$

The above concept is explained by shear stress and normal stress in faults in three different directions, as shown in Fig. 10 (c). The Fig. 10 (c) can be regarded as a case of strike-slip fault, where $\sigma_2 = \sigma_v$. In this case, the ratio of maximum to minimum effective principal stress, namely σ_1 / σ_3, is limited by the frictional strength of the primary fault. For the faults represented by the number 1, if S_1 increases with respect to S_3, sliding occurs when the frictional strength of the faults in the critical direction is reached. Once faults begin to slide, S_1 will no longer increase. This type of faults become critical stress faults that are in a critical state of sliding, while other faults are not. The normal stress of faults that are almost perpendicular to S_1 is relatively large, but the shear stress is small, not enough to cause sliding; while the normal stress and shear stress of the faults almost parallel to S_1 are smaller.

Fault friction strength is the maximum static friction force before fault sliding under the action of *in situ*

stress. *In situ* stress controls the type and nature of the fault and affects the friction strength of fault (Kim and Hosseini, 2017). The original rock stress in the rock mass is a three-dimensional stress field with unequal pressure. The magnitude and direction of the three principal stresses vary with space and time. According to the Anderson's fault theory (Anderson, 1951), there are three types of stress states including normal faults, reverse faults, and translational faults. The upper limit value of the ratio of the maximum to minimum effective principal stresses is estimated as follows:

$$\left.\begin{array}{ll} \text{Normal fault:} & \dfrac{\sigma_1}{\sigma_3}=\dfrac{S_v-P_p}{S_{hmin}-P_p}\le[(\mu^2+1)^{1/2}+\mu]^2 \\ \text{Reverse fault:} & \dfrac{\sigma_1}{\sigma_3}=\dfrac{S_{Hmax}-P_p}{S_v-P_p}\le[(\mu^2+1)^{1/2}+\mu]^2 \\ \text{Strike slip fault:} & \dfrac{\sigma_1}{\sigma_3}=\dfrac{S_{H\max}-P_p}{S_{h\min}-P_p}\le[(\mu^2+1)^{1/2}+\mu]^2 \end{array}\right\} \tag{16}$$

According to Eq. (16) and the three states of the original rock stress of the Anderson fault theory, the lower limit value of the minimum horizontal principal stress of the normal fault and the upper limit value of the maximum horizontal principal stress of the reverse fault and the strike-slip fault are obtained.

$$\left.\begin{array}{ll} \text{Normal fault:} & \sigma_h^{LB}=\dfrac{\sigma_v-P_p+q_fP_p}{q_f} \\ \text{Reverse fault:} & \sigma_H^{UB}=(\sigma_{hmin}-P_p)q_f+P_p \\ \text{Strike slip fault:} & \sigma_H^{UB}=(\sigma_{hmin}-P_p)q_f+P_p \end{array}\right\} \tag{17}$$

Where q_f=$[(\mu^2+1)^{1/2}+\mu]^2$, σ_h^{LB} and σ_H^{UB} are the lower limit of the minimum horizontal principal stress and the upper limit of the maximum horizontal principal stress, respectively.

In the stress mechanism that forms a normal fault, the minimum horizontal principal stress is located between the lower limit of the minimum horizontal stress and the overlying rock load. The *in situ* stresses of S5 borehole and S9 borehole in Xinji No.1 mine are controlled by F10 normal fault, and the minimum horizontal principal stress should be between the lower limit of the minimum horizontal stress and overburden stress. Friction coefficient of F10 fault measured in laboratory μ=0.6 (Ben-David et al., 2010), the lower limit of the minimum horizontal stress can be calculated from Eq. (16), as shown in Fig. 16. It can be seen from Fig. 11 that the magnitude of the minimum horizontal principal stress in this area can be determined by the lower limit value of the minimum horizontal stress when the fault friction coefficient is 0.6.

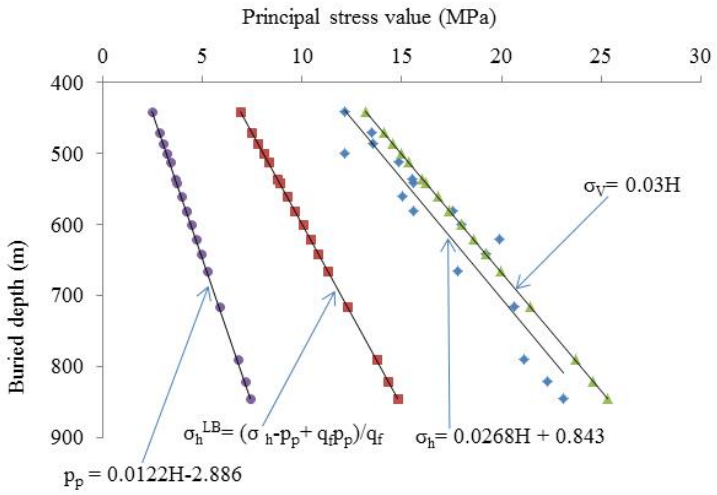

Fig. 16. Relationship between minimum horizontal principal stress and its lower limit and overburden stress in Xinji No. 1 mine.

7. Conclusions

(1) The results of *in situ* stress measurement by hydraulic fracturing method in Xinji No.1 mine showed that the maximum horizontal principal stress ranges from 13.95MPa to 25.23 MPa, the minimum horizontal principal stress was in the range of 12.16-21.17 MPa, and the average azimuth of the maximum horizontal principal stress was N83.61 °E. The magnitude and direction of the same kind of ground stress vary at different points, but there was no mutation, indicating that the ground stress field of the mining area was relatively uniform.

(2) The *in situ* stress in Huainan mining area was dominated by horizontal tectonic stress. Generally, it belonged to the type of tectonic stress field, which was characterized by $\sigma_H > \sigma_v > \sigma_h$. The coal-bearing strata in the Huainan mining area were in a high stress level.

(3) The horizontal and vertical principal stresses increased approximately linearly with the increase of depth. The value of the lateral pressure coefficient (λ) was 0.505 - 1.822, and tended to approach 1.0 as the depth increases. The lateral pressure coefficient of most measuring points in the mining area was greater than 1.0, which reflected that the *in situ* stress state in the mining area was dominated by horizontal stress. The lateral pressure ratio (k) varies in the range of 0.485 - 1.535 and it is rather scattered in the study area. with the increase of the burial depth, the dispersion range of lateral pressure ratio (k) gradually decreases and the value approaches 1.0.

(4) The *in situ* stress field of Huainan mining area basically inherited the *in situ* stress field of the third Cenozoic Himalayan tectonic movement. The maximum principal stress was in the NEE-EW direction. Assuming that the friction coefficient μ of F10 fault in Xinji No. 1 mine is 0.6, the lower limit value of the minimum

horizontal principal stress is approximately determined. Minimum horizontal principal stress value is between its lower limit and vertical stress.

Data Availability

The data used to support the findings of this study are available from the corresponding author upon request.

Conflicts of Interest

The authors declare that they have no conflicts of interest.

Acknowledgements

This study is supported by the National Natural Science Foundation of China (Nos. 41904118, 42072204), Henan Province Scientific and technological research project (No. 202102310218) and the Open Fund of the State Key Laboratory of Water Resource Protection and Utilization in Coal Mining (No. SHJT-17-42.8) and the Key Project of Coal-based Low-carbon Joint Research Foundation of NSFC and Shanxi Province (No. U1910204). We also thank reviewers and editors for their constructive comments and suggestions on improving the manuscript.

References

Anderson, E. M., 1951. The dynamics of faulting and dyke formation with applications to Britain. Hafner Pub. Co.

Archie, G. E., 1950. Introduction to Petrophysics of Reservoir Rocks. AAPG Bulletin, 34(5):943-961.

Bell, J.S., 2006. In-situ stress and coal bed methane potential in Western Canada. Bulletin of Canadian Petroleum Geology. 54(3):197-220.

Ben-David, O., Rubinstein, S., Fineberg, J.2010. Slip-stick and the evolution of frictional strength. Nature 463, 76–79.

BROWN, E.T., HOEK, E., 1978. Trends in relationships between measured in-situ stresses and depth. International Journal of Rock Mechanics and Mining Sciences & Geomechanics Abstracts.15(2): 211-215.

Byerlee, J., 1978. Friction of rocks. Pure & Applied Geophysics. 116(4-5):615-626.

Carder, D.S., 1945. Seismic investigations in the Boulder Dam area, 1940-1944, and the influence of reservoir loading on local earthquake activity. Bulletin of the Seismological Society of America. 4:175-192.

Coggan, J., Gao, F., Stead, D., et al., 2012. Numerical modelling of the effects of weak immediate roof lithology on coal mine roadway stability. International Journal of Coal Geology.90:100-109.

Cornet, F.H., Valette, B., 1984. In situ stress determination from hydraulic injection test data. Journal of Geophysical Research Solid Earth. 89(B13):11527-11537.

Finkbeiner, T., Barton, C.A., Zoback, M.D., 1997. Relationships among in-situ stress, fractures and faults, and fluid flow: Monterey formation, Santa Maria Basin, California. AAPG Bulletin. 81(12):1975-1999.

Funato, A., Ito, T., 2017. A new method of diametrical core deformation analysis for in-situ stress measurements. International Journal of Rock Mechanics and Mining Sciences. 91:112-118.

Gay, N.C., 1975. In-situ stress measurements in Southern Africa. Tectonophysics. 29(1):447-459.

Greiner, G., 1975. In-situ stress measurements in Southwest Germany. Tectonophysics.29(1):265-274.

Guo, H., Yuan, L., Shen. B.T., et al, 2012. Mining-induced strata stress changes, fractures and gas flow dynamics in multi-seam longwall mining. International Journal of Rock Mechanics & Mining Sciences. 54: 129-139.

Haimson, B. C., Fairhurst, C., 1969. In-situ stress determination at great depth by means of hydraulic fracturing. Am. Soc. Mech. Eng. (Pap.); (United States).

Haimson, B. C., 1978. Effect of cyclic loading on rock, In: Dynamic geo-technical testing. ASTM STP 654, Am. Soc. Testing and Materials, 228–245.

Han, J., Zhang, H.W., Song, W.H., et al., 2008. In-situ stress field of coal and gas outburst mining area. Chinese Journal of Rock Mechanics and Engineering. 27(Supp.2): 3852-3859 (In Chinese).

Hubbert, M.K., & Willis, D.G., 1957. Mechanics of hydraulic fracturing. Petroleum transactions, the American institute of mining. Metal., Petrol. Eng. 210, 153-168.

Hoek, E., 1990. Estimating Mohr-Coulomb friction and cohesion values from the Hoek-Brown failure criterion. International Journal of Rock Mechanics and Mining Science & Geomechanics Abstracts. 27(3):227-229.

Kang, H., Zhang, X., Si, L., et al., 2010. In-situ stress measurements and stress distribution characteristics in underground coal mines in China. Engineering Geology. 116(3):333-345.

Kim, S., Hosseini, S. A., 2017. Study on the Ratio of Pore-Pressure/Stress Changes During Fluid Injection and Its Implications for CO2 Geologic Storage. Journal of Petroleum science and Engineering. 149:138-150.

Jaeger, J.C., 1971. Friction of rocks and stability of rock slopes. Geotechnique,21(2): 97-134.

Li, G., Ma, F., Guo, J., et al, 2019. Study on deformation failure mechanism and support technology of deep soft rock roadway. Engineering Geology. 264:105-112.

Li, G.Q., Yan, D.T., Zhuang, X.G., 2019. Implications of the pore pressure and in situ stress for the coalbed methane exploration in the southern Junggar Basin, China. Engineering Geology. 262. 105305.

Li, S. C., Wang, Q., Wang, H. T., et al, 2013. Model test study of surrounding rock deformation and failure mechanism of deep roadway with thick top coal. Tunnelling and Underground Space Technology. 47:52-63.

Li, Z.Y., Yang, Y.Y., 1999. Introduction to engineering geology. China University of Geosciences Press, Wuhan (In Chinese).

Liu, Q.S., Liu, K.D., 2012. Characteristics of in-situ stress field for deep levels in Huainan coal mine． Rock and Soil

Mechanics. 2012，33(7): 2089-2096 (In Chinese).

Logan, J.M., Dengo, C.A., Higgs, N.G., et al., 1992. Fabrics of experimental fault zones: Their development and relationship to mechanical behavior. International Geophysics. 51:33-67.

Martin, C.D., Lanyon, G.W., 2003. Measurement of in-situ stress in weak rocks at Mont Terri Rock Laboratory, Switzerland. International Journal of Rock Mechanics & Mining Sciences. 40(7–8):1077-1088.

Meng, Z., Zhang, J., Wang, R., 2011. In-situ stress, pore pressure and stress-dependent permeability in the Southern QinshuiBasin. International Journal of Rock Mechanics & Mining Sciences. 48(1):122-131.

Oliver, H., Mojtaba, R., Xiaofeng, C., et al., 2018. The world stress map database release 2016: crustal stress pattern across scales. Tectonophysics. 744, 484-498.

Paul, S., Chatterjee, R., 2011. Mapping of cleats and fractures as an indicator of in-situ stress orientation, Jharia coalfield, India. International Journal of Coal Geology. 88(2):113-122.

Peng, X.F., Yu, S.Z., 1998. General type of in-situ stress Field in Huainan mine area. Journal of China University of Mining & Technology.27(1):60-63 (In Chinese).

Shan, Z., Yan, P., 2010. Management of rock bursts during excavation of the deep tunnels in Jinping II Hydropower Station. Bull Eng Geol Environ. 69, 353–363.

Xiao, Y.X., Feng X.T., Li, S.J., et al.,2016. Rock mass failure mechanisms during the evolution process of rockbursts in tunnels. International Journal of Rock Mechanics & Mining sciences.83:174-181.

Yaghoubi, A.A., Zeinali, M., 2009. Determination of magnitude and orientation of the in-situ stress from borehole breakout and effect of pore pressure on borehole stability-Case study in Cheshmeh Khush oil field of Iran. Journal of Petroleum Science & Engineering. 67(3-4):116-126.

Yang, J., Chen, W., Zhao, W., et al., 2017. Geohazards of tunnel excavation in interbedded layers under high in situ stress. Engineering Geology. 230:11-22.

Yang, W., Lin, B. Q., Zhai. C., et al., 2012. How in situ stresses and the driving cycle footage affect the gas outburst risk of driving coal mine roadway[J]. Tunnelling & Underground Space Technology, 31:139-148.

Zhao, X.G., Wang, J., Qin, X.H., et al., 2015. In-situ stress measurements and regional stress field assessment in the Xinjiang candidate area for China's HLW disposal. Engineering Geology. 197(4): 42-56.

Zoback, M.D, 2007. Reservoir Geomechanics. Cambridge University Press, Cambridge, UK.

Zoback, M.D., Moos, D., Mastin, L., et al., 1985. Well bore breakouts and in situ stress. Journal of Geophysical Research. 90:5523-5530.

Figures

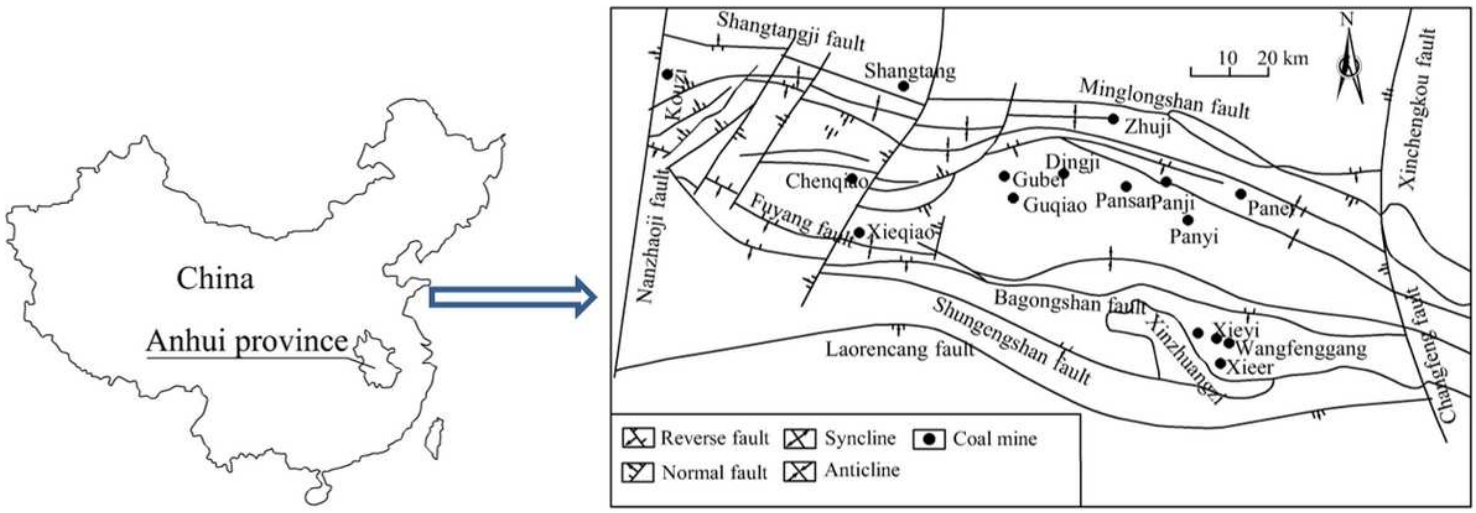

Figure 1

Geological structure diagram of the Huainan mining area in Anhui province. Note: The designations employed and the presentation of the material on this map do not imply the expression of any opinion whatsoever on the part of Research Square concerning the legal status of any country, territory, city or area or of its authorities, or concerning the delimitation of its frontiers or boundaries. This map has been provided by the authors.

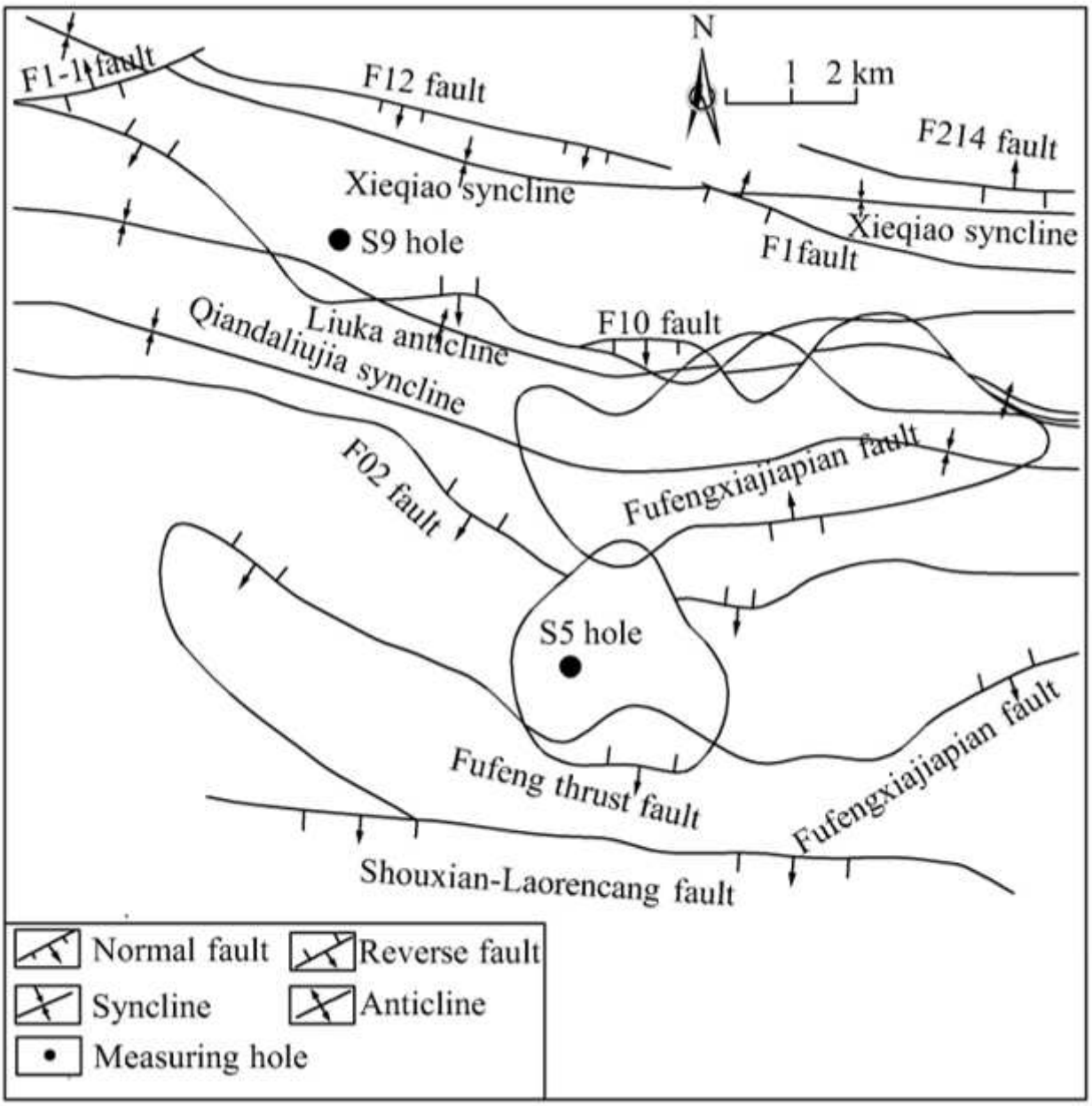

Figure 2

Geological structure in the Xinji No.1 coal mine.

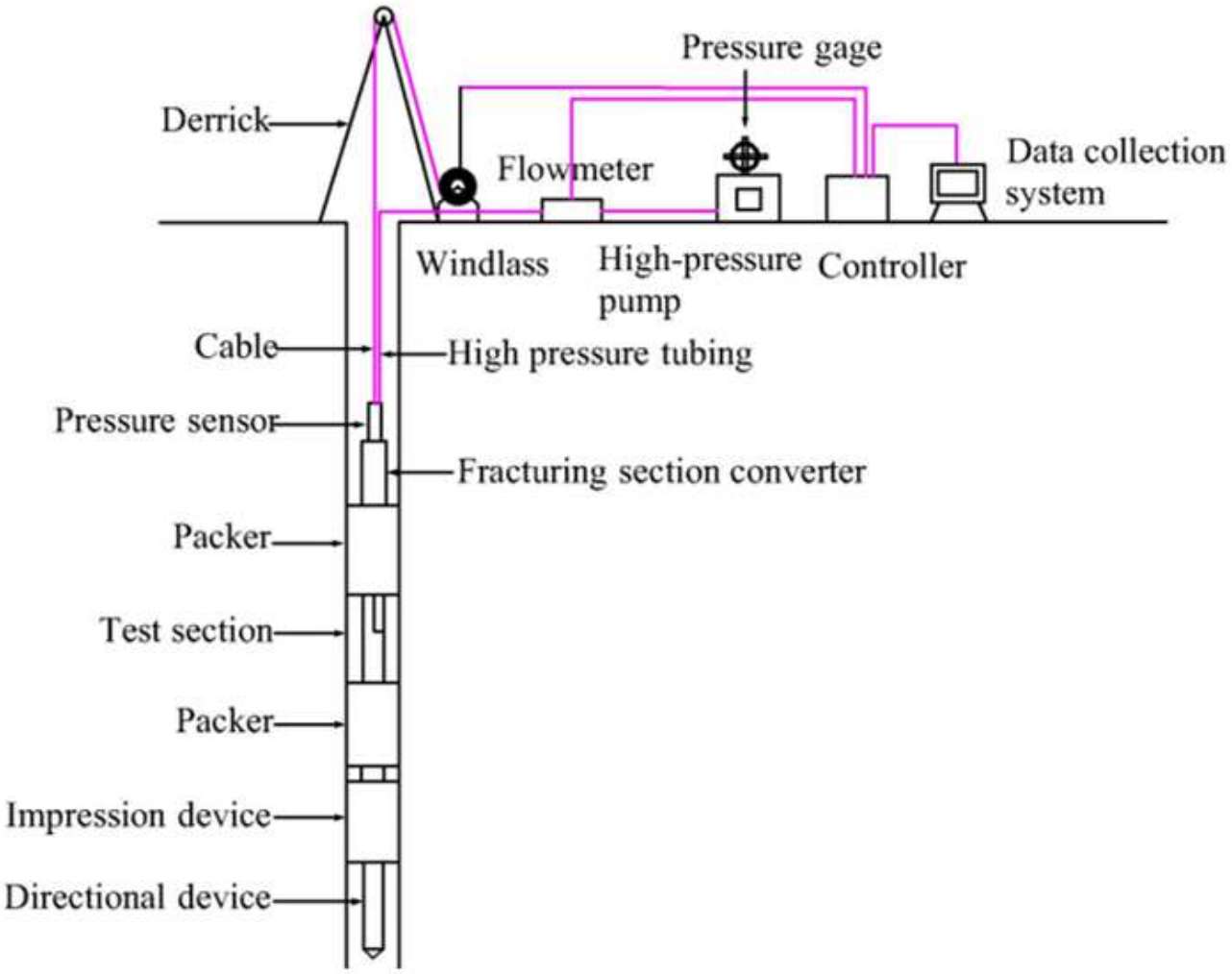

Figure 3

Sketch of single loop hydraulic fracturing in situ stress measurement system.

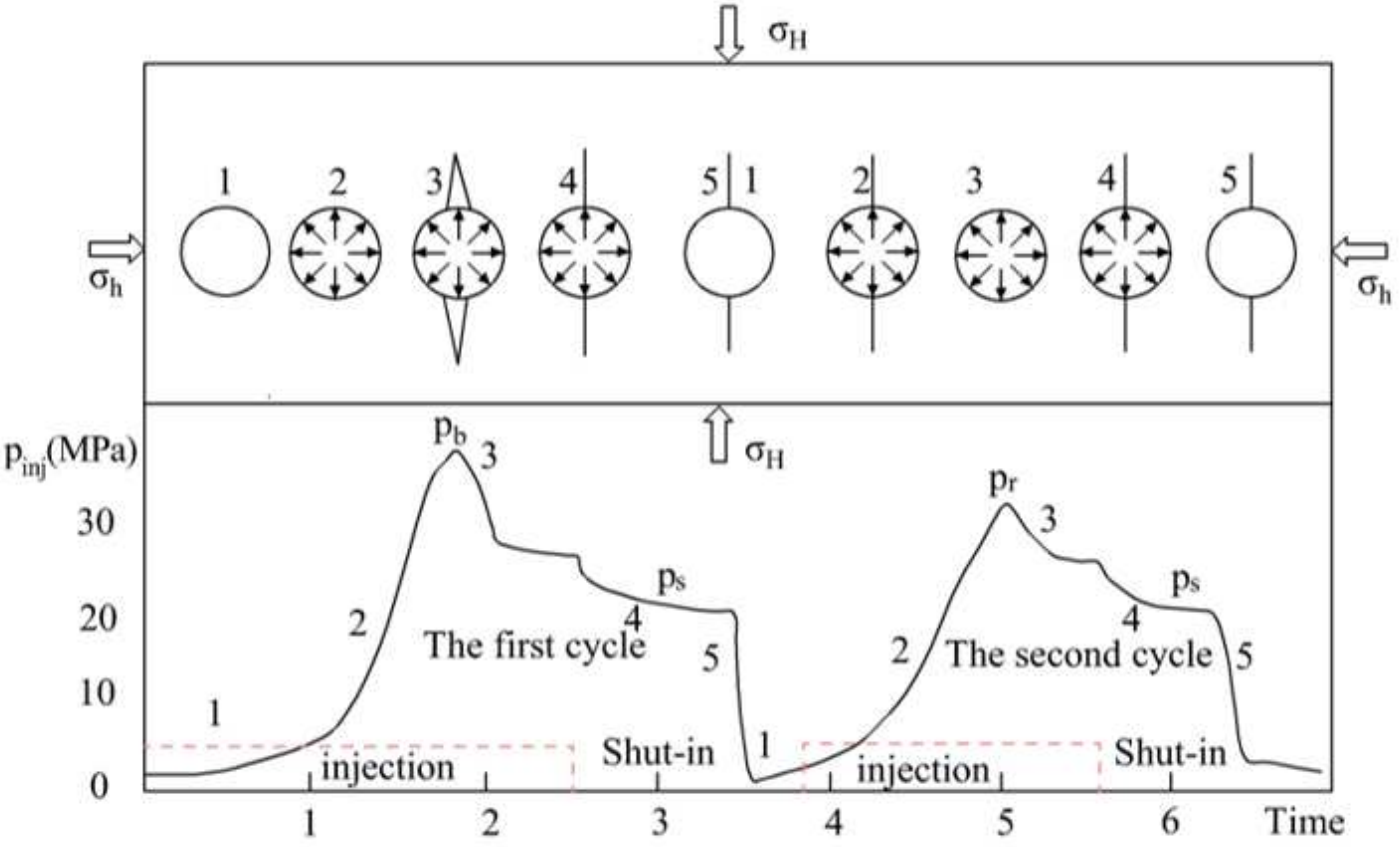

Figure 4

Typical fracturing process curve of hydraulic fracturing stress measurement.

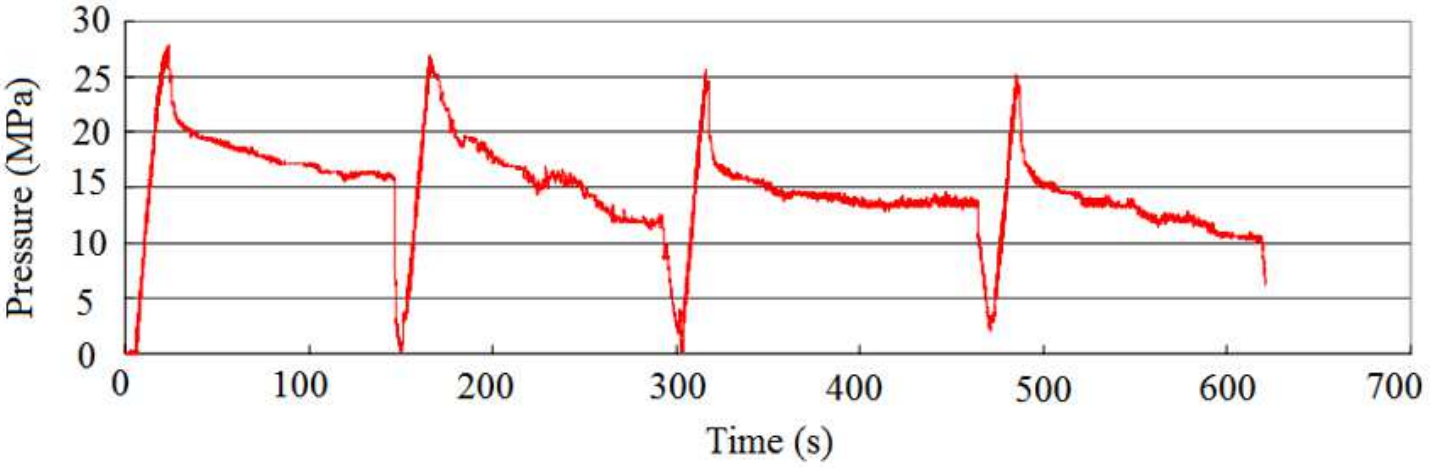

Figure 5

Pumping pressure versus test time at the depth of 439.5-440.5 m in S5 hole.

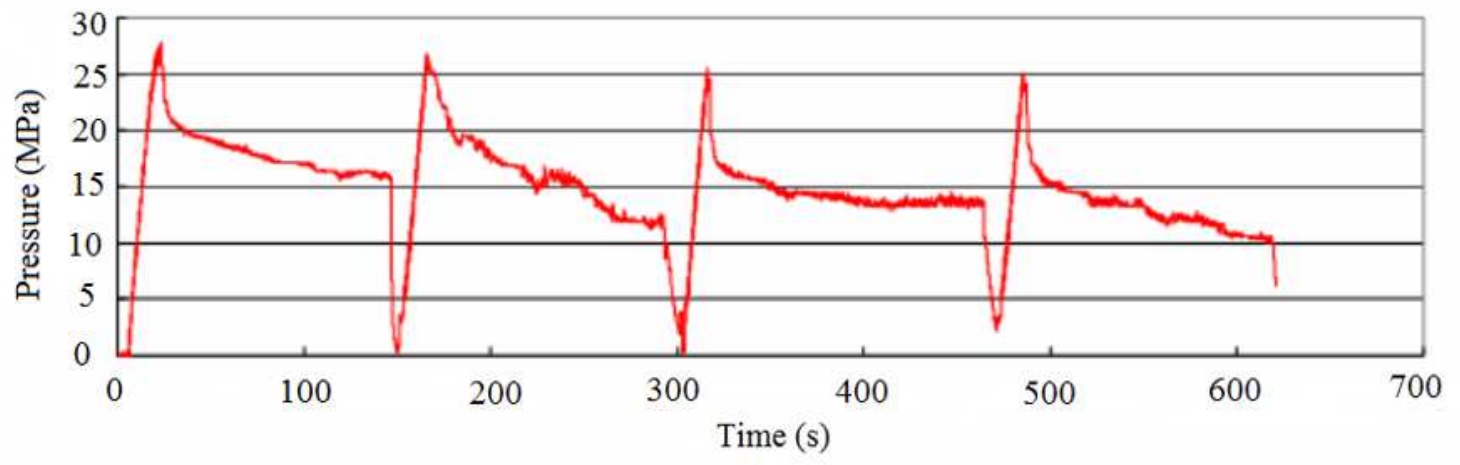

Figure 6

Pumping pressure versus test time at the depth of 539.5-540.5 m in S5 hole.

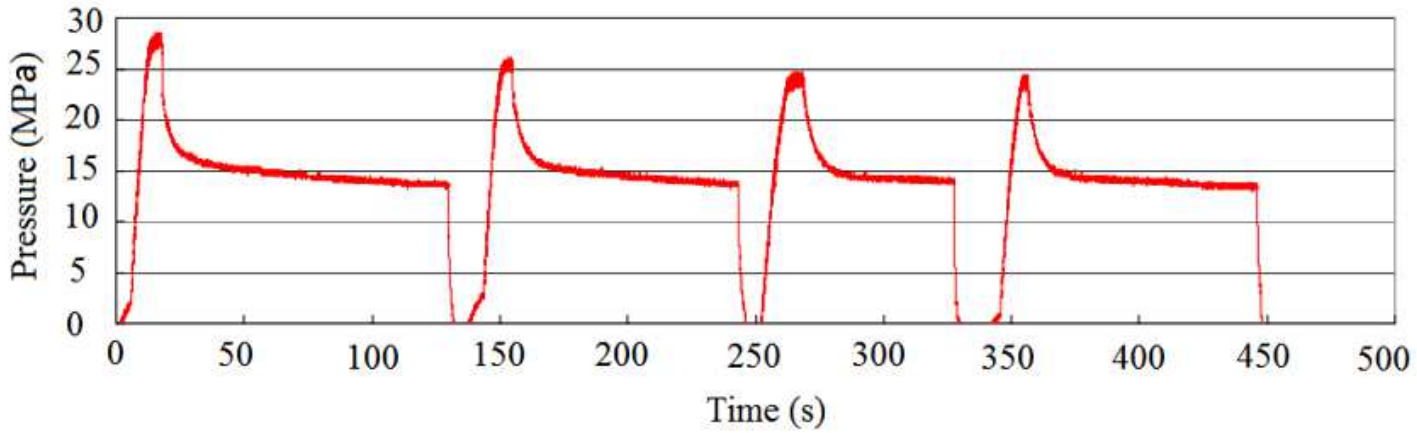

Figure 7

Pumping pressure versus test time at the depth of 664.5-665.5 m in S9 hole.

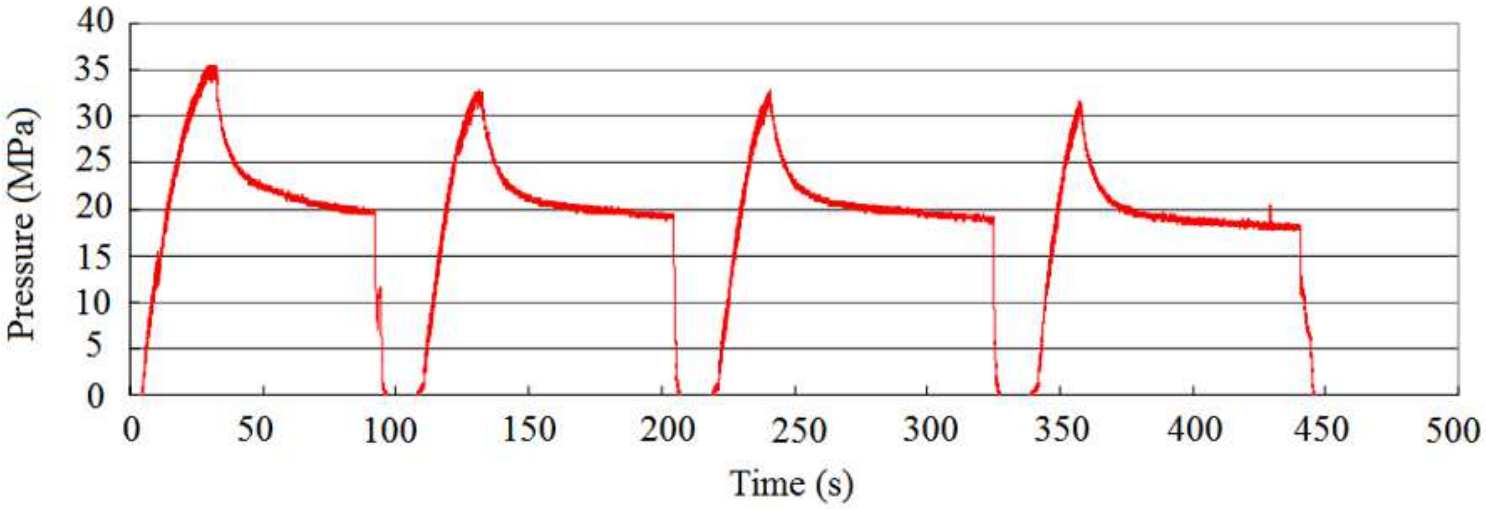

Figure 8

Pumping pressure versus test time at the depth of 789.5-790.5 m in S9 hole.

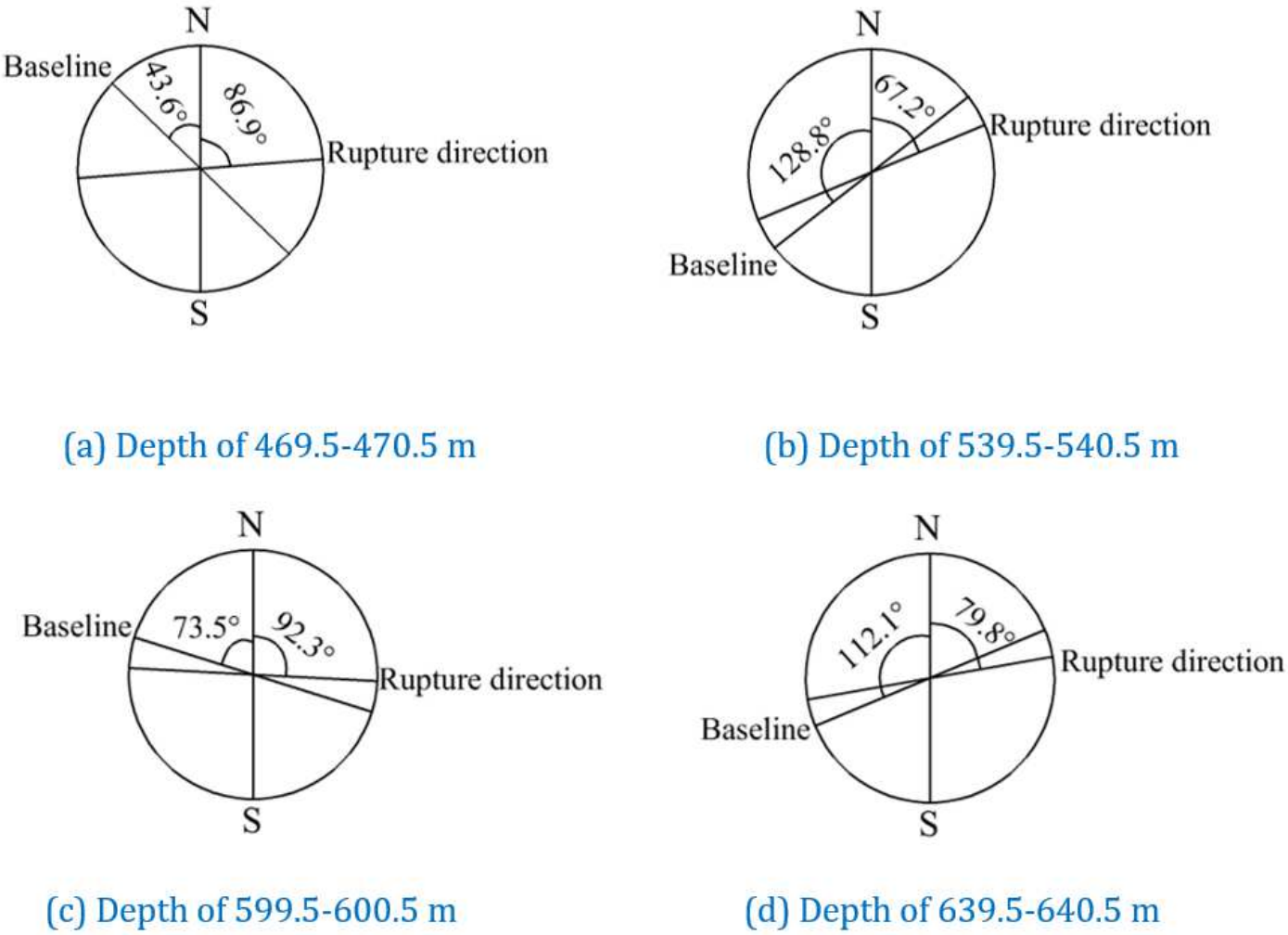

Figure 9

Orientations of the observed hydraulic fractures in Hole S5 injection test in four depth intervals.

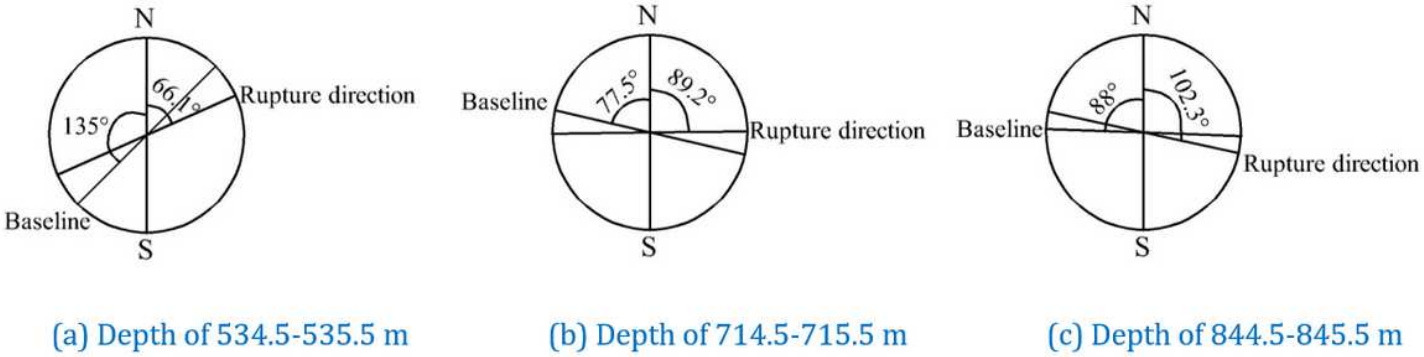

Figure 10

Orientations of the observed hydraulic fractures in Hole S5 injection test in four depth intervals.

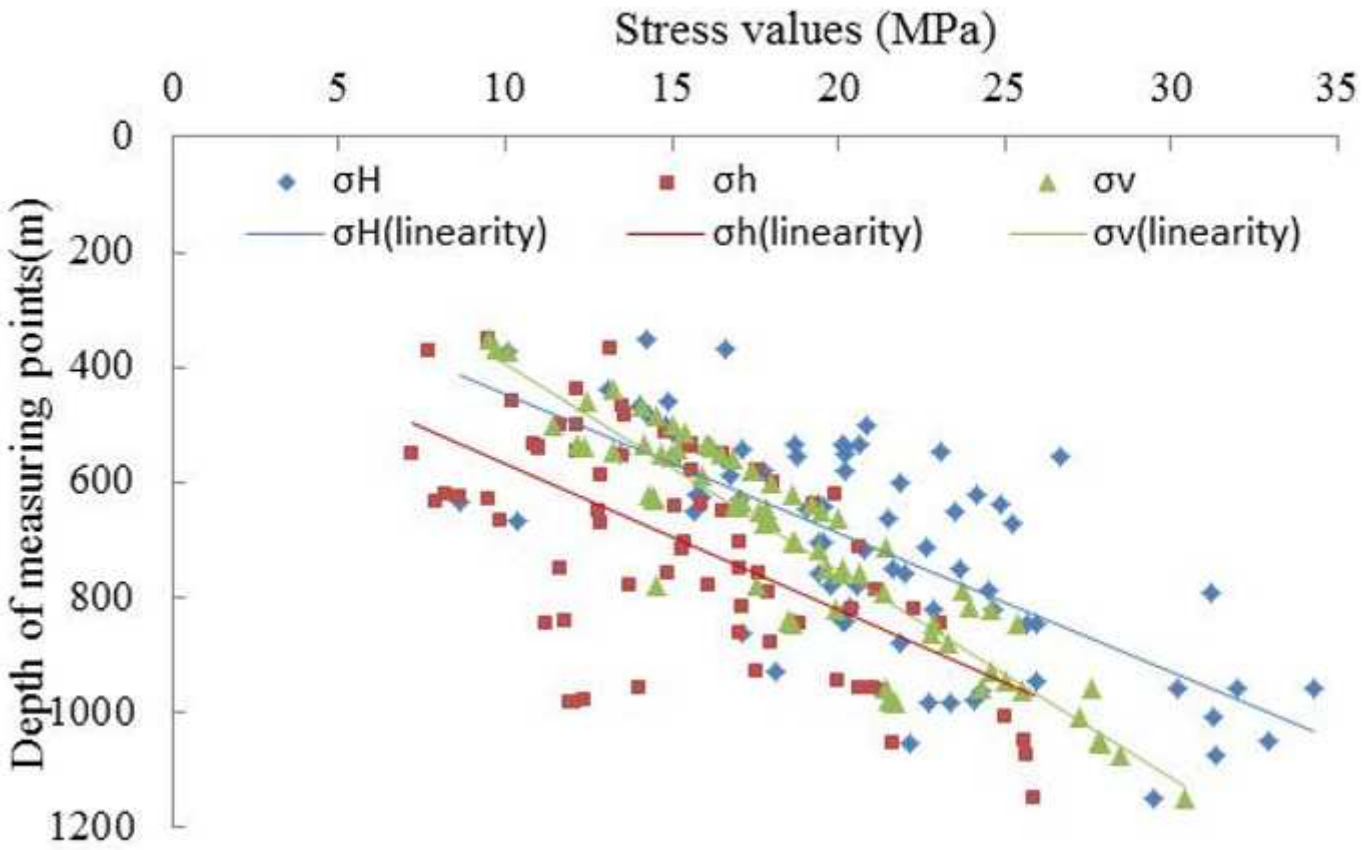

Figure 11

Variation of in situ stress values with depth in Huainan mining area.

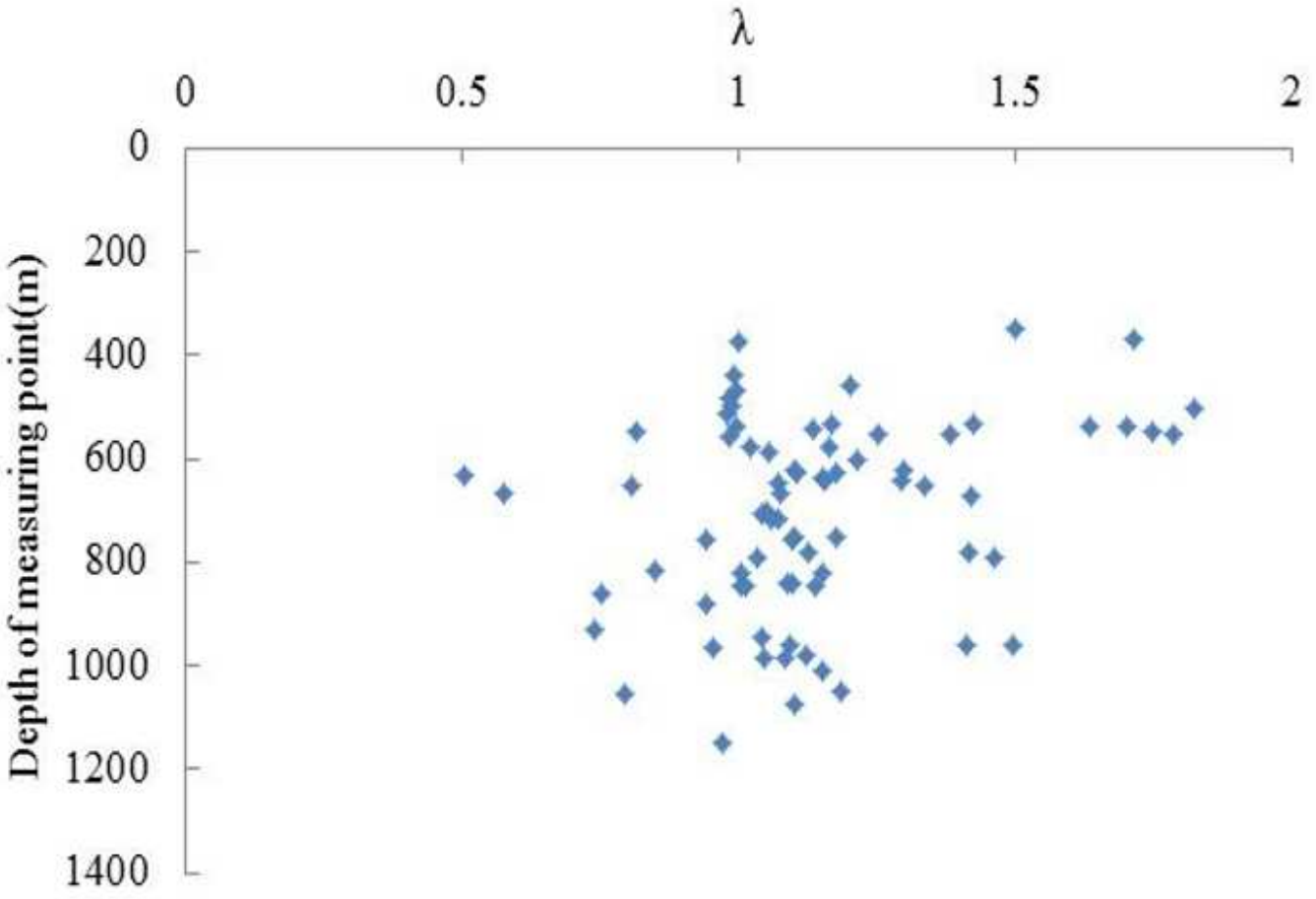

Figure 12

Ratio of minimum horizontal principal stresses to vertical principal stresses with depth.

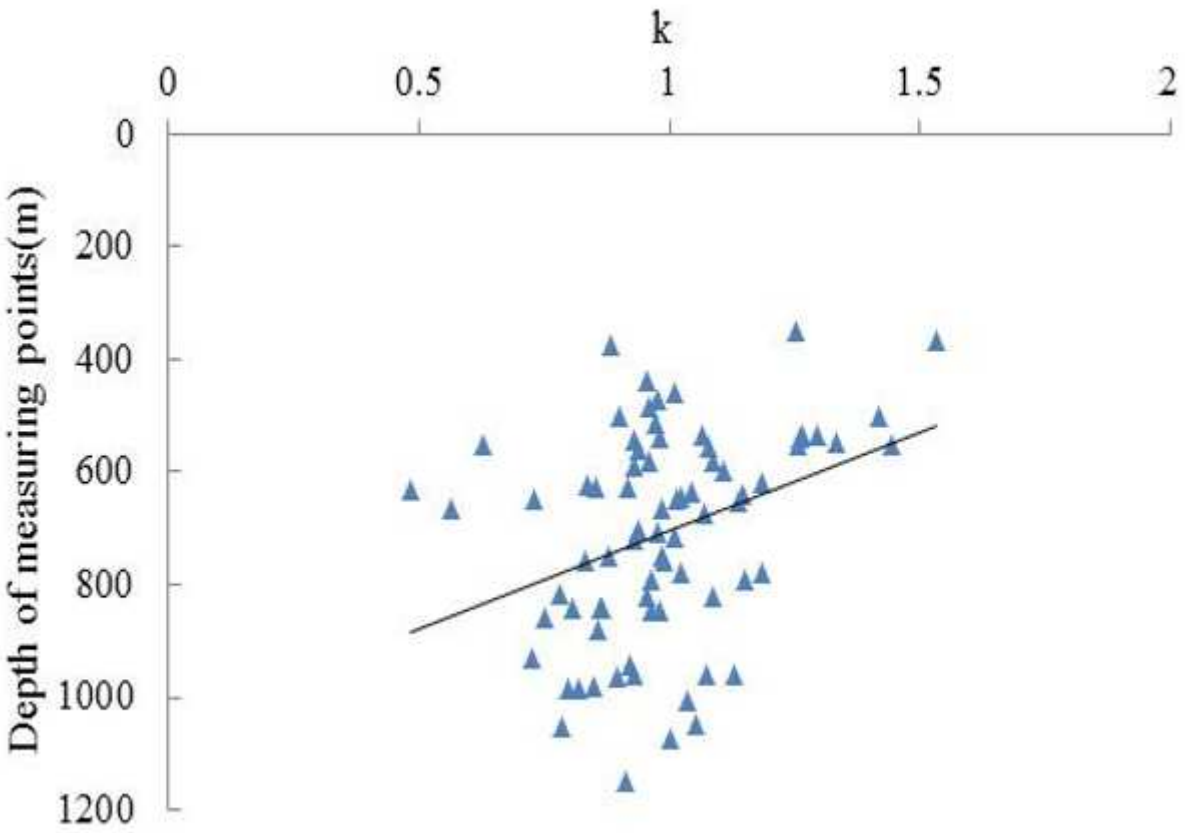

Figure 13

Ratio of average horizontal principal stress to vertical stress vs depth.

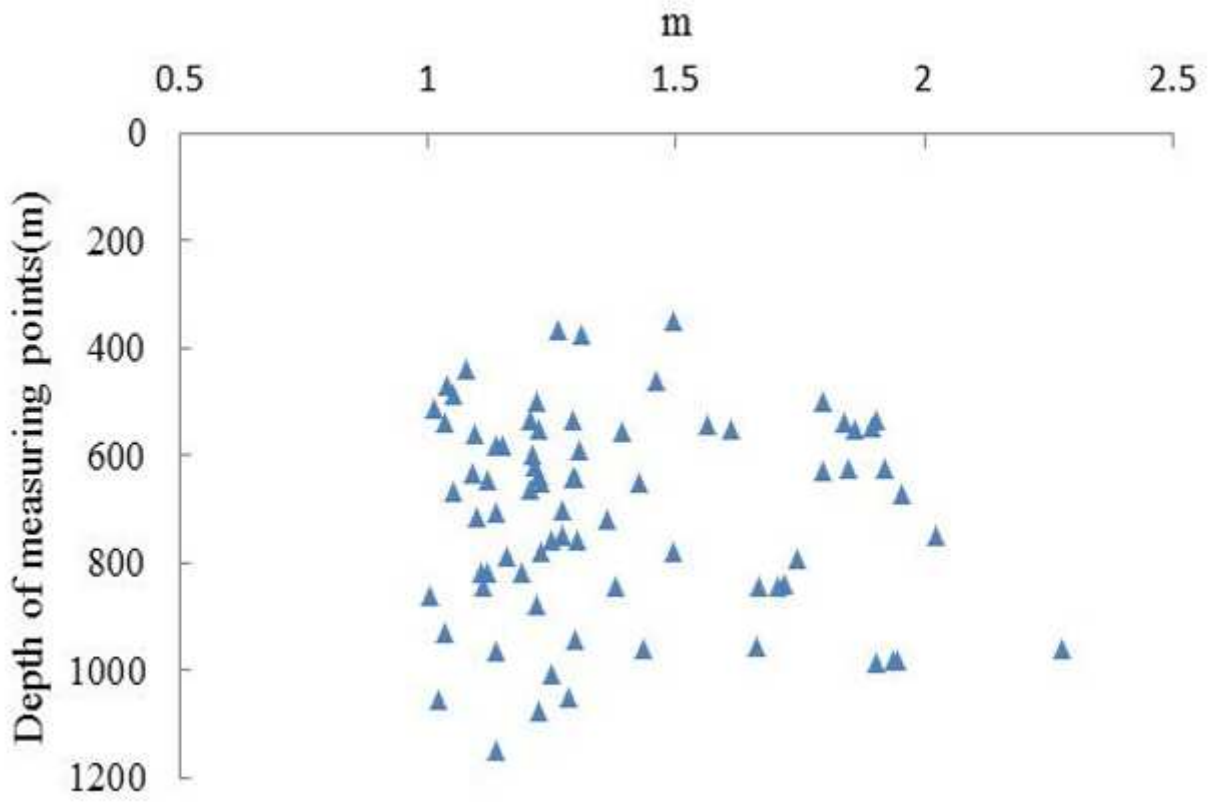

Figure 14

The ratio of maximum to minor horizontal principal stress varying with depth.

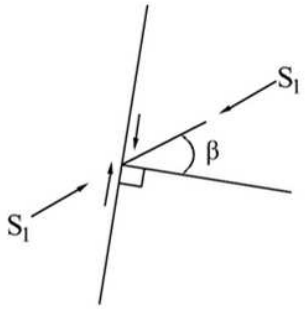

(a) Fault slip occurred in the dominant direction.

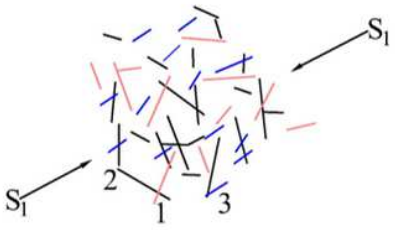

(b) There are faults in various directions in the formation, and some of them are in the dominant direction where sliding occurs.

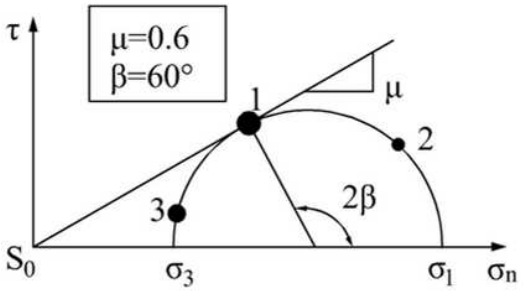

(c) Mohr circles for faults in different directions.

Figure 15

Limiting diagram of fault frictional strength on in situ stress.

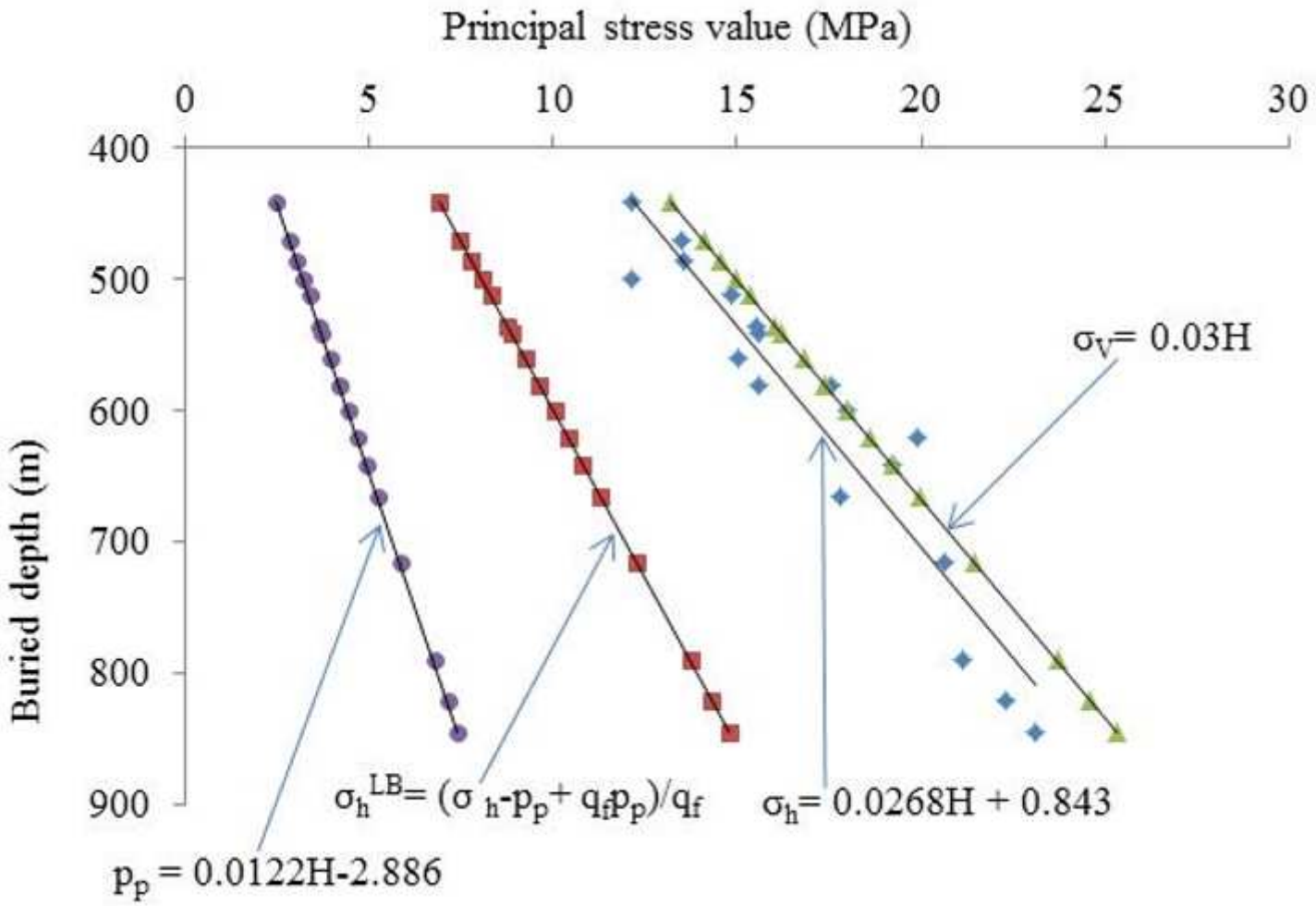

Figure 16

Relationship between minimum horizontal principal stress and its lower limit and overburden stress in Xinji No. 1 mine.